

# 000 001 002 003 004 005 006 007 008 009 010 011 012 013 014 015 016 017 018 019 020 021 022 023 024 025 026 027 028 029 030 031 032 033 034 035 036 037 038 039 040 041 042 043 044 045 046 047 048 049 050 051 052 053 HIERARCHICAL INSTRUCTION-AWARE EMBODIED VISUAL TRACKING

Anonymous authors

Paper under double-blind review

## ABSTRACT

User-centric embodied visual tracking (UC-EVT) requires embodied agents to follow dynamic, natural language instructions specifying not only which target to track, but also how to track—including distance, angle, and directional constraints. This dual requirement for robust language understanding and low-latency control poses significant challenges, as current approaches using end-to-end RL, VLM/VLA, and LLM-based methods fail to adequately balance comprehension with low-latency tracking. In this paper, we introduce **Hierarchical Instruction-aware Embodied Visual Tracking (HIEVT)**, which decomposes the problem into on-demand instruction understanding with spatial goal generation (high-level) and asynchronous continuous goal-conditioned control execution (low-level). HIEVT employs an *LLM-based Semantic-Spatial Goal Aligner* to parse diverse human instructions into spatial goals that directly specify desired target positioning, coupled with an *RL-based Adaptive Goal-Aligned Policy* that enables real-time target positioning according to generated spatial goals. We establish a comprehensive UC-EVT benchmark using over 1.7 million training trajectories, evaluating performance across one seen environment and nine challenging unseen environments. Extensive experiments and real-world deployments demonstrate HIEVT’s superior robustness, generalizability, and long-horizon tracking capabilities across diverse environments, varying target dynamics, and complex instruction combinations. The complete project is available at <https://sites.google.com/view/hievt>.

## 1 INTRODUCTION

Providing Human-Computer Interaction has become increasingly appealing for modern intelligent robots and downstream applications (Zuo et al., 2025; Olaiya et al., 2025; Hoffman et al., 2024; Wu et al., 2025; Pueyo et al., 2024). We introduce **User-Centric Embodied Visual Tracking (UC-EVT)** task, an extension of the previous Embodied Visual Tracking Task (EVT), as users demand more dynamic and interactive systems beyond fixed targets and distance (Van Toan et al., 2023; Zhang et al., 2023). In particular, users expect systems that can respond effectively in dynamic and complex scenarios (Li et al., 2023; Zhou et al., 2024; Ma et al., 2023), quickly comprehend instructions and adapt to new assigned targets, varying in appearance, speed and expected angle of view, without restarting to modify tracking parameters or switch targets. Motivated by the above needs, this paper proposes three core requirements for UC-EVT: **1) User Instructions Understanding.** The UC-EVT agent must be capable of interpreting user instructions, such as natural language commands, to dynamically adjust the tracking agent, including targets, angles, and distances. **2) Real-Time Responsiveness.** The agent must operate in real time, maintaining robust performance while receiving continuous instructions or switching to different targets in dynamic environments. **3) Flexibility and**

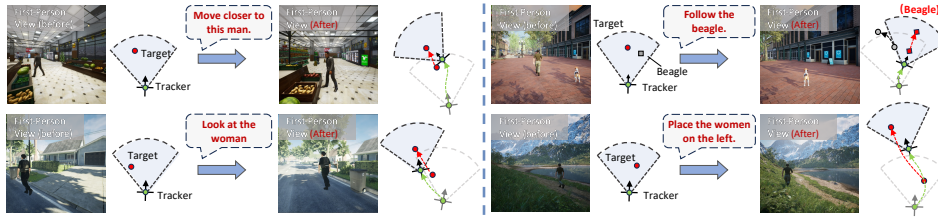


Figure 1: Examples of User-Centric embodied visual tracking with diverse instructions.

054 **Generalizability.** The agent should flexibly adapt to targets with various appearances and speeds,  
 055 unseen scenarios, diverse instructions, and evolving spatial relationships, without retraining.  
 056

057 Existing methods (Luo et al., 2019; Zhong et al., 2019b; 2021; 2023; Wang et al., 2025) primarily  
 058 focus on **Embodied Visual Tracking (EVT)** task, aiming to maintain a stable distances or angles  
 059 relative to a target by adjust its tracking behaviors. Reinforcement learning (RL)-based models,  
 060 for example, utilize the distance from the target to the expected location (usually at the center of  
 061 the view) as the reward to train tracking policy in an end-to-end manner (Luo et al., 2019; Zhong  
 062 et al., 2019b; 2021). Further, reasearchers leverage vision foundation models (Zhong et al., 2024) to  
 063 facilitate the domain gap. Recently, systems like Vision-Language-Action Models (VLA) (Kim et al.,  
 064 2024; Wang et al., 2025) and general-purpose large models (e.g., LLMs and VLMs) have demonstrate  
 065 the capability on EVT task while maintain the comprehension ability at same time.

066 Despite these advancements, existing methods face significant limitations when applied to UC-EVT  
 067 tasks: **1) Limited Comprehension and Flexibility in RL-based EVT:** RL-based EVT models  
 068 struggle to handle complex user instructions and exhibit poor transferability across different envi-  
 069 ronments and embodiments. Their rigid tracking strategies (e.g., fixed distances or angles) hinder  
 070 adaptability to user-centric instructions. **2) Limited Generalization of VLA Models:** VLA models  
 071 rely heavily on large-scale annotated data, making them ill-suited for unseen conditions such as novel  
 072 environments, instructions, targets, or agents. **3) Inference Latency in Large Models:** While large  
 073 models exhibit strong capabilities, their inference speeds (typically 0.5–3 FPS) are insufficient for  
 074 real-time tracking, resulting in frequent target loss during fast movements.

075 To address these limitations, we propose a **Hierarchical Instruction-aware Embodied Visual**  
 076 **Tracking (HIEVT)** agent that integrates instruction comprehension models with adaptive tracking  
 077 policies and introduces intermediate spatial goals to bridge human instructions and agent behavior.  
 078 Specifically, we introduce an *LLM-based Semantic-Spatial Goal Aligner*, serving as a high-level  
 079 planning module, translating diverse instructions into explicit spatial goals, complement for the  
 080 insufficiency of comprehension while maintaining spatial precision. The low-level *RL-Based Adaptive*  
 081 *Goal-Aligned Policy* modeling temporoal spatial information and explicit spatial goals at same image  
 082 space, enhancing the agent’s generalization on diverse target speed while preserve a precise tracking  
 083 approximate to the expected spatial goal. Meanwhile, the low-level policy integrate the vision  
 084 foundation models (VFM) to faciliate task irrelevant visual features, ensuring the learned policy is  
 085 category-agnostic. Our hierarchical design follows a asynchronous updating mechanism, the low-level  
 086 policy continuously tracking given the latest goal generated from high-level module without blocking  
 087 on LLM/VLM inference, ensuring a balance of semantic reasoning and real-time performance.

088 Our contributions are summarized as follows: 1) We introduce the User-Centric Embodied Visual  
 089 Tracking (UC-EVT) task, which lays the foundation for user-centric human-robot interactions, en-  
 090 abling robots to follow users and provide personalized services. 2) We propose a novel Hierarchical  
 091 Instruction-aware EVT (HIEVT) model that effectively addresses the limitations of state-of-the-art  
 092 (SOTA) models while preserving their advantages. 3)We establish a comprehensive UC-EVT bench-  
 093 mark by extending public EVT benchmark with instruction-based tracking, variable target speeds, 10  
 094 diverse environments, over 1.7M annotated trajectories, and competitive baselines including classical  
 095 control, RL policies, and SOTA VLA/VLM models. 4) Our comprehensive experiments evaluate  
 096 the HIEVT’s superiority in terms of general tracking performance, dynamic instruction adaptation,  
 097 generalization ability, and real-time responsiveness in both simulation and real-world transferability.

## 098 2 RELATED WORKS

099 **Embodied Visual Tracking (EVT)** is a foundational skill of embodied AI. Early EVT systems  
 100 (Yoshimi et al., 2006; Ye et al., 2023; Müller & Koltun, 2021) often relied on passive visual feature  
 101 extractors combined with handcrafted controllers such as PID or Kalman filters to drive the robot to-  
 102 ward the target. While these approaches achieved basic tracking functionality, they lacked robustness  
 103 in cluttered or dynamic environments and could not flexibly adapt to different tracking objectives  
 104 or user demands. To improve robustness and generalisation in complex environments, recent EVT  
 105 research has shifted toward reinforcement learning (RL)-based method (Zhong et al., 2019a; 2021).  
 106 Recent work Zhong et al. (2024) combines the visual foundation model (Cheng et al., 2023a) and  
 107 offline reinforcement learning to improve the training efficiency and generalization of the tracker.  
 108 However, these methods train the agent to track at a specific relative position to the target. If we need

108 to change the goal, fine-tuning the policy network is required to adapt to new goals. This limits the  
 109 flexibility and applicability of the agents across varied scenarios and tasks.  
 110

111 **Instruction-aware Robot** is developed to complete tasks by understanding and following human  
 112 instructions, bridging the gap between high-level human intentions and low-level robotic actions.  
 113 Early works such as Touchdown (Chen et al., 2019) and R2R (Anderson et al., 2018) focused on  
 114 vision-language navigation in real-world environments. Subsequent efforts leveraged large pre-trained  
 115 models to fuse multimodal instructions and enhance generalization. For instance, PALM-E (Driess  
 116 et al., 2023) builds on a large language model for embodied reasoning, AVLEN (Paul et al., 2022)  
 117 incorporates audio and natural language in 3D navigation, and VIMA (Jiang et al., 2022) uses  
 118 multimodal prompts for systematic generalization. While recent VLA paradigm like TrackVLA  
 119 (Wang et al., 2025) shows that VLAs can be extended to EVT, it still exhibits limited generalization to  
 120 unseen target categories and various dynamics. Furthermore, these models cannot accurately follow  
 121 fine-grained user instructions that require precise spatial placement of the target, which is essential  
 122 in UC-EVT. These limitations highlight the need for a hierarchical framework that integrates the  
 123 reasoning strength of large models with the real-time responsiveness of lightweight control policies.  
 124

### 3 HIERARCHICAL INSTRUCTION-AWARE EMBODIED VISUAL TRACKING

125 In this section, we present the design insight of our proposed model, **Hierarchical Instruction-aware**  
 126 **Embody Visual Tracking (HIEVT)**. The core challenge of the User-Centric Embodied Visual  
 127 Tracking (UC-EVT) is the giant gap from the user instruction  $\mathcal{I}_t$  and the actual state  $\mathcal{S}_t$  of the tracker.  
 128 Moreover, the instruction  $\mathcal{I}_t$  is given by a user-friendly mode rather than an agent-friendly mode. To  
 129 bridge the gap, it is necessary to import an intermediate goal  $\mathcal{G}_{inter}(t)$  to bridge the user's instruction  
 130 and the agent's state. This decomposition allows for user instruction understanding as well as efficient  
 131 agent decision-making, formulated as:  
 132

$$\mathcal{D}(\mathcal{I}_t, \mathcal{S}_t) \approx \underbrace{\mathcal{D}(\mathcal{I}_t, \mathcal{G}_{inter}(t))}_{\text{Semantic-Spatial Goal Aligner}} + \underbrace{\mathcal{D}(\mathcal{G}_{inter}(t), \mathcal{S}_t)}_{\text{Adaptive Goal-Aligned Policy}}, \quad (1)$$

133 where  $\mathcal{D}(\mathcal{I}_t, \mathcal{G}_{inter}(t))$  represents the distance between the user instruction and the intermediate  
 134 goal, and  $\mathcal{D}(\mathcal{G}_{inter}(t), \mathcal{S}_t)$  represents the distance between the intermediate goal and the agent state.  
 135 We then detail the design of the key components, LLM-based Semantic-Spatial Goal Aligner and  
 136 RL-based Adaptive Goal-Aligned Policy, the entire model structure is illustrated in Figure 2. At  
 137 inference time, our system adopts **asynchronous processing** between goal generation and policy  
 138 execution. When the Semantic-Spatial Goal Aligner receives a new instruction, it may incur variable  
 139 latency due to LLM inference or communication delays. Rather than blocking the control loop, the  
 140 system maintains a continuous and stable tracking by using the recent available spatial goal  $\mathcal{G}_*$ . This  
 141 design ensures the adaptive goal-aligned policy runs smoothly without pausing (up to 50 fps with  
 142 lightweight VFM configuration), while the goal aligner operates at its own pace. This asynchronous  
 143 architecture decouples slow semantic reasoning from fast control, enabling both rich instruction  
 144 understanding and real-time control.  
 145

#### 3.1 LLM-BASED SEMANTIC-SPATIAL GOAL ALIGNER

146 The Semantic-Spatial Goal Aligner (SSGA) is the fundamental component responsible for translating  
 147 diverse user instructions  $\mathcal{I}_t$  to a spatial goal  $\mathcal{G}_{inter}(t)$ . Given the input user instruction  $\mathcal{I}_t$ , the  
 148 SSGA outputs an intermediate goal  $\mathcal{G}_{inter}(t) = (\mathcal{C}_t, G_t)$ , where  $\mathcal{C}_t$  is the target category, and  
 149  $G_t^* = [x_t, y_t, w_t, h_t]$  is a spatial goal, representing the expected target's spatial position in the  
 150 bounding box format. The SSGA consists of three core components:  
 151

152 **Semantic Parsing** The first step in SSGA is to interpret the user instruction  $\mathcal{I}_t$  and extract critical  
 153 information for goal specification: the target category  $\mathcal{C}_t$ . This process is performed by the semantic  
 154 parser  $\mathcal{C}_t = \mathcal{P}_{sem}(\mathcal{I}_t)$ , where  $\mathcal{C}_t \in \mathcal{T}$  indicates the target attributes. For instance, given the instruction  
 155 “Get closer to the blue car” the semantic parser identifies  $\mathcal{C}_t = \{\text{“blue car”}\}$ .  
 156

157 **Spatial-Goal Generation** To resolve ambiguities in user instructions, our parser grounds its inter-  
 158 pretation of input instruction  $\mathcal{I}_t$  in both linguistic context and visual features. This dual-grounding  
 159 approach enables robust semantic alignment between natural language commands and environmental  
 160

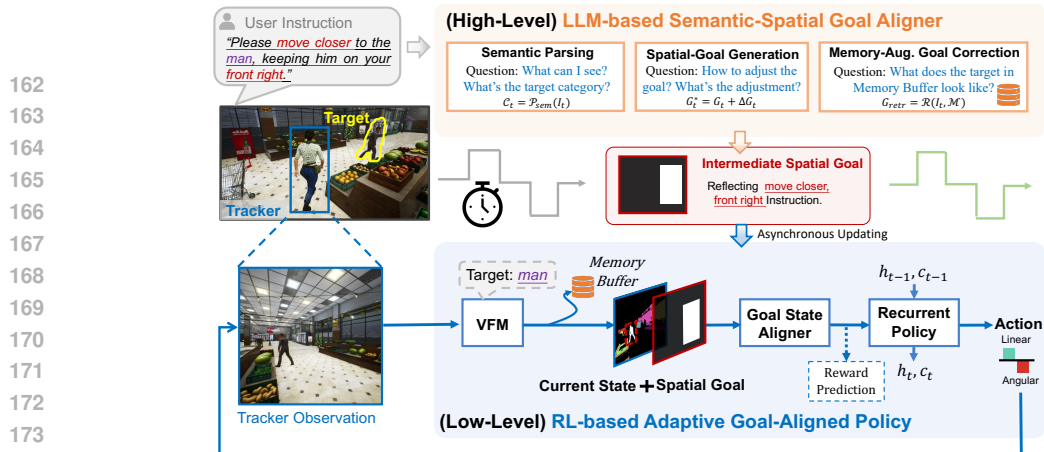


Figure 2: Overview of the Hierarchical Instruction-aware Embodied Visual Tracker (HIEVT). Given a natural language instruction and environmental observation, our system first processes the instruction through the LLM-based Semantic-Spatial Goal Aligner including Semantic Parsing, Spatial-Goal Generation, and Memory-Augmented Goal Correction. This produces a target attribute and a bounding box format spatial goal. The RL-based Adaptive Goal-Aligned Policy then combines this goal with the Visual Foundation Model (VFM) processed observation, feeds them into the following policy network. The Goal State Aligner and Recurrent Policy then generate appropriate action signals to maintain the desired spatial relationship with the target.

observations. Through this process, the parser generates a spatial goal representation  $G_t^*$  that accurately reflects the intended spatial directives. This is achieved using a chain-of-thought (COT)-based reasoning mechanism Wei et al. (2022), which incrementally adjusts the current target’s spatial representation  $G_t$ . The spatial goal generation process is formulated as:

$$G_t^* = G_t + \Delta G_t, G_t = \mathcal{B}(\mathcal{VFM}(\mathcal{O}_t, \mathcal{C}_t)) \quad (2)$$

where  $\mathcal{VFM}(\mathcal{O}_t, \mathcal{C}_t)$  uses Vision Foundation Models (VFs) to extract text-conditioned segmentation mask with target-highlighted format given the target category name Zhong et al. (2024),  $\mathcal{B}(\cdot)$  detects target’s bounding box from segmentation mask by filtering the target’s corresponding mask color (white color),  $\Delta G_t = [\Delta x_t, \Delta y_t, \Delta w_t, \Delta h_t]$  represents the adjustment to the current target’s spatial representation. The adjustment is determined by  $\Delta G_t = \mathcal{F}_{COT}(\mathcal{I}_t, G_t)$ , where  $\mathcal{F}_{COT}$  represents a chain-of-thought reasoning process implemented through a large language models. This reasoning process interprets how the spatial directive in instruction  $\mathcal{I}_t$  should modify the current observed target’s spatial representation  $G_t$ , producing adjustment parameters  $\Delta G_t$  for both position and size. To guide this interpretation, we developed a system prompt that structures the model’s reasoning, ensuring it correctly analyzes spatial relationships (provided in supplementary materials) and translates natural language instructions into geometric transformations. The COT-based approach ensures that the bounding box adjustments are interpretable and aligned with the user’s intent, allowing for dynamic and context-aware reasoning about the spatial relationship.

**Memory-Augmented Goal Correction** After generating the spatial goal  $G_t^*$ , the SSGA applies a correction step using a memory-augmented generation (RAG) mechanism. This step ensures that the generated bounding box is consistent with trajectory priors stored in a memory buffer  $\mathcal{M}$ . The RAG module retrieves similar instructions and their corresponding bounding boxes from  $\mathcal{M}$ , i.e.,  $G_{retr} = \mathcal{R}(\mathcal{I}_t, \mathcal{M})$ , where  $\mathcal{R}$  is the retrieval function (i.e. Cosine similarity). The retrieved spatial goal  $G_{retr}$  is then used for determining if the generated goal  $G_t^*$  satisfies the target’s physical constraints (e.g., aspect ratio or perspective effect). If conflicts arise, specifically, the Intersection over Union (IoU) (Leal-Taixé et al., 2015; Cordts et al., 2016) value is lower than a threshold (Appendix F.2), the historical mask is used as the final spatial goal  $G_t^*$ :

$$G_t^* = \begin{cases} G_t^*, & \text{IoU}(G_t^*, G_{retr}) > 0.5 \\ G_{retr}, & \text{IoU}(G_t^*, G_{retr}) \leq 0.5 \end{cases} \quad (3)$$

This correction mechanism combines the adaptability of COT-based reasoning with the consistency of target physical constraints, ensuring robust and accurate bounding box predictions.

216 3.2 RL-BASED ADAPTIVE GOAL-ALIGNED POLICY  
217

218 The proposed Adaptive Goal-Aligned Policy (AGAP) module bridges the intermediate goal  $\mathcal{G}_{inter}(t)$   
219 and the user implied state  $\mathcal{S}_t$ , ensuring precise alignment of the agent’s actions with user instructions.  
220 This alignment is achieved by an adaptive motion policy which dynamically adjust the agent’s move-  
221 ment based on the observation  $\mathcal{O}_t$  towards the spatial position indicated by  $\mathcal{G}_{inter}(t)$ . We leverage  
222 VFM-generated mask, to generalize across diverse target objects, as the mask-based representation  
223 mitigates domain gaps in texture and appearance variations. The adaptive policy is optimized using  
224 offline reinforcement learning with an auxiliary reward regression task to facilitate the alignment,  
225 formulated as:  $\pi(a_t | G^*, \mathcal{O}_t)$ . Below, we elaborate on the key components of this module.  
226

227 **Architecture** The policy consists of two main components: 1) Goal-State Aligner contains mul-  
228 tiple convolutional neural network (CNN) layers, serving as the feature extraction and alignment  
229 module. It encodes VFM-extracted binary masks highlighting target regions and the spatial goal  
230 representation at image-level space, where the mask-based encoding provides appearance-agnostic  
231 features that enable generalization to unseen target categories. This aligner outputs a latent aligned  
232 representation. Then, a reward prediction layer follows the aligner, serving as the auxiliary task to  
233 improve the aligned ability in a self-supervised manner. 2) Recurrent Policy Network consists of a  
234 long short-term memory (LSTM) network that models the temporal dynamics of the tracking process  
235 to enhance the spatial-temporal consistency of the representation and an actor network  $V_\phi$ . Moreover,  
236 the LSTM’s temporal modeling capability enables speed generalization by learning motion patterns  
237 across varying target velocities during training. The latent representation from the Goal-state aligner  
238 was fed to the LSTM network, followed by the Actor Network to generate motion control action  $a_t$ .  
239 More details about the networks are in supplementary materials.  
240

241 **Goal-conditioned Offline Policy Optimization** For Adaptive Goal-Aligned Policy (AGAP), our  
242 aim is to train a policy that can adapt to diverse spatial goals and achieve precise and fast alignment.  
243 Traditional Online RL methods are typically designed for a single-goal objective, and require a  
244 huge amount of trial-and-error to converge. Therefore, we use the offline reinforcement learning  
245 (Offline-RL) paradigm to train the goal-conditioned policy, considering the training efficiency and  
246 dataset diversity’s contribution to the overall performance. Meanwhile, we introduce an auxiliary  
247 regression task to improve the alignment ability. Below, we detail the reward design, offline-RL  
248 training objectives and the auxiliary regression task.

249 *Training Data Preparation.* We extend the data collection procedure in Zhong et al. (2024) to  
250 incorporate a broader range of goal conditions, as the generalization capabilities of our frame-  
251 work critically depend on trajectory diversity. Our dataset  $\mathcal{D}$  consists of trajectories  $\mathcal{T}_t =$   
252  $(\mathcal{S}_t, \mathcal{O}_t, a_t, r_t, \mathcal{O}_{t+1}, \mathcal{S}_{t+1}, G_t^{final})$ , where  $t$  is the time step,  $\mathcal{S}_t$  and  $\mathcal{O}_t$  represent the tracker’s state  
253 and observation,  $a_t$  and  $r_t$  denote the action and IoU-based reward, and  $G_t^{final}$  specifies the spatial  
254 goal. For each episode, we randomly sample goals within the tracker’s field of view to ensure diverse  
255 spatial configurations, with relative distances  $\rho_t \in (200, \rho_{max})$  and angles  $\theta_t \in (-\theta_{max}/2, \theta_{max}/2)$ . A  
256 state-based PID controller with injected noise perturbations generates the goal-conditioned tracking  
257 trajectories, enhancing variability and robustness. The final training dataset comprises 10 million  
258 steps.

259 *IoU-based Training Reward.* The reward function  $r_t$  is designed to guide the policy move toward  
260 aligning  $\mathcal{O}_t$  with  $G_t^{final}$ . At each time step  $t$ , the reward is defined as:

$$261 \quad r_t = \text{IoU}(G_t^{final}, \mathcal{B}(\mathcal{V}\mathcal{F}\mathcal{M}(\mathcal{O}_t, \mathcal{C}_t))), \quad (4)$$

263 where higher values of Intersection over Union (IoU) indicate the agent is moving towards better  
264 alignment in the 2D image.  
265

266 *Offline Reinforcement Learning.* In this paper, inspired by previous works (Zhong et al., 2024), we  
267 extend the standard offline RL algorithms, Conservative Q-Learning (CQL) (Kumar et al., 2020),  
268 adapting to goal-conditioned setting. Specifically, we use two critic networks  $Q_\theta^1, Q_\theta^2$  to estimate  
269 goal-conditioned Q values. The Q-functions are updated by minimizing the following objective:  
 $L_\theta = \sum_{G=1}^N L_G$ , where the objective consists of the sum of the losses from all sampled goals in the

270 batch, with each goal’s loss computed according to the following formula:  
 271

$$272 \quad L_G = \mathbb{E}_s \left[ \log \sum_a \exp Q_\theta^i(s, a) - \mathbb{E}_{a \sim \pi_\phi(a|s)} [Q_\theta^i(s, a)] \right] \\ 273 \\ 274 \\ 275 \quad + \frac{1}{2} \mathbb{E}_{s, a, s'} \left[ (Q_\theta^i(s, a) - (r + \gamma \mathbb{E}_{a' \sim \pi_\phi} [Q_{min}(s', a') - \alpha \log \pi_\phi(a' | s')])^2 \right] \quad (5) \\ 276$$

277 where  $\theta$  and  $\phi$  are network parameters,  $\alpha$  is the entropy regularization coefficient which controls the  
 278 degree of exploration.  $i \in \{1, 2\}$ ,  $Q_{min} = \min_{i \in \{1, 2\}} Q_\theta^i$ ,  $\gamma$  is the discount factor,  $\pi_\phi$  is the learned  
 279 policy that derived from the actor network  $V_\phi$ . Note that the state-goal aligner and the recurrent  
 280 policy are jointly optimized by the RL loss.

281 *Auxiliary Reward Regression.* For the goal-state aligner, we introduce an auxiliary reward regression  
 282 task during training to facilitate the alignment between the goal and state representations. This task  
 283 encourages the agent to recognize high-reward states associated with different goals, effectively  
 284 steering the learned action policy toward these states. Specifically, we incorporate a fully connected  
 285 layer following the goal-state aligner, predicting the alignment reward  $\hat{r}_t$ , the alignment loss is  
 286 computed using  $L_{reg} = \text{MSE}(r_t, \hat{r}_t)$ , where MSE denotes the mean squared error, the gradients are  
 287 only updated to the goal-state aligner. Note that, the output of the fully connected layer will not be  
 288 fed to the recurrent policy network, which will not affect inference stage.

## 289 4 EXPERIMENT

290 In this section, we conduct comprehensive experiments in virtual environments and real-world  
 291 scenarios, aiming to address the following **five** questions: Q1) Can HIEVT outperform state-of-the-art  
 292 models on tracking performance, robustness, and generalizability? Q2) How does the adjusting  
 293 precision and efficiency of HIEVT when there is a new instruction? Q3) How do HIEVT and baselines  
 294 perform under different target moving speeds and dynamic target category switches? Q4) How do  
 295 key components of HIEVT affect its performance? Q5) How does HIEVT perform in real world?

### 297 4.1 EXPERIMENTAL SETUP

298 **Environments.** We evaluate our approach across 10 virtual environments that extend from previous  
 299 EVT benchmark (Zhong et al., 2017; 2024), including FlexibleRoom for training, and rest for testing,  
 300 as shown in Figure 5. These environments span urban, confined, industrial, and architectural settings  
 301 with varied challenges. Please refer to the Appendix D for detailed introduction.

302 **Instruction Set Creation.** To evaluate UC-EVT, we construct an instruction set that includes  
 303 *sequential instructions* and *target-switch instructions*. Specific details can be found in Appendix F.1.  
 304 For sequential instructions, we parse the comma-separated sub-instructions and input each subsequent  
 305 sub-instruction at 120-step intervals during trajectory execution, achieving continuous instruction  
 306 input throughout the trajectory. For target-switch instructions, since animals perform random walks  
 307 in the environment, we utilize the environment’s absolute information to detect when animals enter  
 308 the field of view and trigger the corresponding instruction input accordingly.

309 **Evaluation Metric.** Our ultimate goal is to realise the flexibility and versatility of embodied visual  
 310 tracking and enable more natural human-robot interactions through our hierarchical aligned agents.  
 311 Therefore, we keep the consistency with the task definition, assessing our method’s ability given  
 312 diverse textual instructions. In the experiment, we call the UnrealCV API to obtain the tracker’s  
 313 real-time spatial position  $(\rho_t, \theta_t)$  and calculate the reward corresponding to different instructions,  
 314 formulated as:  $r(I_t, s_t) = 1 - \frac{|\rho_t - \rho_t^*|}{\rho_{max}} - \frac{|\theta_t - \theta_t^*|}{\theta_{max}}$ , where  $(\rho_{max}, \theta_{max})$  are the maximum distance  
 315 and angle within the tracker’s field of view,  $(\rho_t^*, \theta_t^*)$  are spatial goal corresponding to Instruction  $I_t$ .  
 316 We follow the evaluation setting in previous works Zhong et al. (2023; 2024), setting the episode  
 317 length to 500 steps with corresponding termination conditions. We use three evaluation metrics: 1)  
 318 Average Accumulated Reward (AR) calculates the average accumulated reward over 50 episodes,  
 319 indicating overall performance in instruction-behavior alignment; 2) Average Episode Length (EL)  
 320 is the average number of steps across 50 episodes, reflecting long-term tracking performance. 3)  
 321 Success Rate (SR) calculates the percentage of episodes reaching 500 steps in 50 episodes.

322 **Baselines.** To evaluate the tracking performance of our method under instruction settings, we compare  
 323 it with six representative baselines from classical control, reinforcement learning, and large-model

Table 1: Performance comparison across ten environments using sequential instructions as input. Each cell reports Average Accumulated Reward (AR), Average Episode Length (EL), and Success Rate (SR) in the format AR/EL/SR.

Environment	Mask-PID (real-time)			Ensembled RL (real-time)			Word2Vec+RL (real-time)			GPT-4o (<1 FPS)			TrackVLA (8 FPS)			Ours (real-time)		
	AR↑	EL↑	SR↑	AR↑	EL↑	SR↑	AR↑	EL↑	SR↑	AR↑	EL↑	SR↑	AR↑	EL↑	SR↑	AR↑	EL↑	SR↑
FlexibleRoom	154	<u>365</u>	0.50	<u>183</u>	330	0.36	28	357	0.42	15	194	0.10	57	<b>500</b>	<b>1.00</b>	278	500	1.00
Suburb	124	<u>386</u>	0.36	<u>126</u>	294	0.22	-5	182	0.00	14	241	0.20	-46	306	<u>0.30</u>	<u>166</u>	<u>445</u>	<u>0.72</u>
Supermarket	<u>175</u>	298	0.26	114	<u>393</u>	0.38	-6	186	0.00	54	286	0.16	35	337	<u>0.48</u>	<u>212</u>	<u>422</u>	<u>0.64</u>
Parking Lot	112	356	0.38	<u>169</u>	301	0.42	2	192	0.00	23	286	0.30	70	<u>441</u>	<u>0.80</u>	<u>169</u>	<u>491</u>	0.93
Old Factory	<u>80</u>	309	0.30	64	334	0.36	-15	183	0.00	5	297	0.32	22	<u>390</u>	<u>0.60</u>	<u>128</u>	<u>469</u>	0.84
Container Yard	<u>140</u>	369	0.42	27	327	0.24	-28	121	0.00	-43	149	0.00	-43	<u>398</u>	<u>0.60</u>	<u>156</u>	<u>469</u>	0.76
Desert Ruins	<u>128</u>	297	0.26	56	368	0.34	9	182	0.00	-5	249	0.26	56	<u>421</u>	<u>0.72</u>	<u>148</u>	<u>434</u>	0.74
Brass Garden	<u>120</u>	302	0.38	-8	<u>348</u>	0.34	-6	142	0.00	3	243	0.18	-1	324	<u>0.44</u>	<u>126</u>	<u>425</u>	0.72
Old Town	<u>73</u>	305	0.32	14	<u>356</u>	0.32	-12	196	0.00	29	304	0.28	-133	247	0.16	<u>85</u>	<u>433</u>	0.64
Roof City	<u>64</u>	289	0.34	19	<u>322</u>	<u>0.38</u>	-8	173	0.00	18	256	0.20	-60	301	0.36	<u>86</u>	<u>400</u>	0.58
<b>Average (Mean)</b>	<b>117.0</b>	327.6	0.35	76.4	337.	0.34	-4.1	191	0.04	11.3	250	0.20	-4.3	367	<u>0.55</u>	<b>155.4</b>	<b>448.8</b>	<b>0.76</b>
<b>Average (Std)</b>	$\pm 34.0$	$\pm 34.9$	$\pm 0.07$	$\pm 64.1$	$\pm 28.5$	$\pm 0.06$	$\pm 14.2$	$\pm 59.6$	$\pm 0.13$	$\pm 23.8$	$\pm 46.1$	$\pm 0.09$	$\pm 61.7$	$\pm 72.7$	$\pm 0.24$	$\pm 54.8$	$\pm 30.6$	$\pm 0.13$

paradigms: (i) *Mask-PID*: A traditional two-stage tracking paradigm using target masks and a PID controller for spatial goal alignment. (ii) *Ensembled RL Policy*: An extension of the RL-based EVT model (Previous SOTA in ECCV24 Zhong et al. (2024)), where multiple policies are trained for different spatial goals and evaluated using regex-based goal matching. (iii) *Word2Vec+RL*: A variant of Ensembled RL that jointly trains an instruction encoder with a policy network using pretrained Word2Vec embeddings (Mikolov et al., 2013) . (iv) *GPT-4o*: VLM model that generates discrete actions from observed images and natural language instructions through multimodal reasoning. (v) *TrackVLA*: A state-of-the-art VLA-based tracker (Wang et al., 2025) that adapts large vision-language-action models for embodied visual tracking tasks. Details of these baselines are provided in the Appendix G.2.

## 4.2 MAIN RESULTS (Q1)

**Overall Performance** As shown in Table 1, our method achieves the best performance in the FlexibleRoom environment, with a perfect success rate and the highest reward (AR = 278). While TrackVLA also attains a success rate of 1.0, its reward is much lower (AR = 57), reflecting weak alignment despite target retention. Traditional baselines such as Mask-PID , Ensembled RL , and Word2Vec+RL achieve moderate episode lengths but fail to ensure dynamic intention alignment. In contrast, large-model approaches (GPT-4o) suffer from low efficiency and poor responsiveness, leading to significantly degraded tracking.

**Generalization in Unseen Environments** More importantly, our approach maintains robust performance across all nine unseen environments, with success rates ranging from 0.58 (Roof City) to 0.93 (Parking Lot) and episode lengths consistently exceeding 400 steps. This demonstrates strong environmental generalization, in sharp contrast to baselines that degrade severely in unseen settings. Although TrackVLA achieves reasonable tracking in certain environments (e.g., FlexilbeRoom, ParkingLot and Desert Ruins), its performance varies drastically across scenes and reveals weak cross-environment generalization, further underscoring the robustness of HIEVT.

**Baseline Limitations** The comparative analysis reveals distinct failure modes across baselines: (1) Mask-PID benefits from using absolute ground-truth annotations, showing relatively smaller degradation across different environments. However, it still lags far behind HIEVT due to the inherent limitations of regex parsing and PID control. In particular, when the tracking distance or goal changes, the intrinsic oscillatory behavior of PID often causes the target to drift out of view, especially during rapid switches near the frame boundary. (2) Ensemble RL preserves the strengths of RL-based methods (SOTA in ECCV'24), showing good generalization and stability when tracking fixed targets. However, its main limitation lies in handling dynamic goal switches: frequent policy loading incurs inference delays, and temporal feature inconsistency across different policies leads to misalignment between instructions and behavior. (3) GPT-4o, despite strong reasoning capabilities, is constrained by extreme inference latency, resulting in a disastrous performance. (4) TrackVLA, while performing reasonably well in human-centered scenarios, lacks explicit spatial goal representations and shows poor robustness in generalization. It fails to adapt to unseen target categories (Table 3) and quickly degrades under higher target speeds (Table 2), underscoring its limited applicability to UC-EVT;

**Key Advantages** Our approach’s superior performance stems from its spatial goal representation serving as an intermediate abstraction between language and action. This design enables consistent

tracking across diverse environments without requiring environment-specific adaptation, while maintaining real-time performance (50 FPS). The results demonstrate that our framework successfully bridges the gap between natural language instructions and precise spatial tracking behaviors in dynamic, real-world scenarios.

### 4.3 ADAPTABILITY OF THE GOAL-ALIGNED POLICY (Q2)

Figure 3: Pixel-level distance between target center and goal center across time steps. The spike at step #101 represents a goal shift instruction, followed by rapid corrections (steps #107, #112) as our agent adjusts to the new spatial goal.

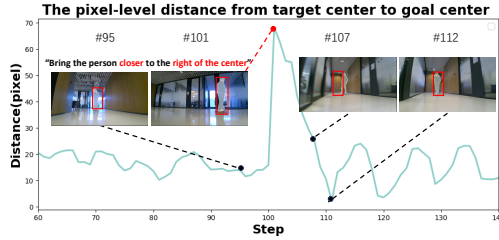


Table 2: **Speed generalization analysis** in FlexibleRoom. Only our method maintains high success rates at high speeds (SR=0.84 at 2.0 m/s) while followed by rapid corrections (steps #107, #112) baselines show severe degradation.

Method	Maximum moving speed of the target		
	0.5 m/s	1.0 m/s	2.0 m/s
Mask-PID	154/365/0.50	-5/330/0.44	-23/125/0.02
Ensembled RL	183/330/0.36	187/313/0.32	-183/208/0.10
Word2Vec+RL	28/357/0.42	21/310/0.36	-56/224/0.12
GPT-4o	15/194/0.10	4/229/0.08	-119/122/0.00
TrackVLA	57/500/1.00	19/431/0.70	-2/287/0.30
Ours	278/500/1.00	274/496/0.98	145/463/0.84

**Precise and Fast Alignment.** To demonstrate HIAEVT’s precise and efficient adaptation to dynamically changed instructions, we visualised a goal-switch case and recorded the pixel-level deviation in real-world deployment. for quality analysis, as shown in Figure 3. When the goal changes at step #101, our system responds with remarkable speed—reducing the pixel distance from 67 to 24 pixels within just 6 steps (#107) and achieving near-perfect alignment (2 pixels) by step #112. This represents complete adaptation within **220ms**. The system maintains this precision through step #127 despite continued target movement, showcasing both initial responsiveness and sustained tracking accuracy. Table 2 further validates this capability across varying target speeds, with our method maintaining a 0.84 success rate even at 2.0 m/s while all baselines fail (0.00-0.30 success rates).

**Real-time inference challenges (Q3)** We tested system robustness by increasing target speeds from  $0.5\text{m/s}$  to  $2.0\text{m/s}$  (Table 2). This experiment reveals a critical real-world challenge: making decisions under real-time constraints. Large-model based methods (TrackVLA, GPT-4o) fail completely at higher speeds (0.30 SR at  $2.0\text{m/s}$ ) due to inference latency (8 FPS, <1 FPS), while conventional approaches (PID, Ensembled RL) degrade significantly ( $0.50 \rightarrow 0.02$  SR,  $0.36 \rightarrow 0.10$  SR). In contrast, our method maintains a high success rate (0.84 SR) even at  $2.0\text{m/s}$ . This demonstrates our hierarchical framework successfully balances semantic understanding with operational efficiency—a crucial capability for real-world deployment where targets move at unpredictable speeds and instructions require immediate responses.

Table 3: **Category generalization.** Four unseen animals were introduced to FlexibleRoom. Results with dynamic target switching

Method	AR	EL	SR
Mask-based PID	152	364	0.52
Ensembled Policy	76	210	0.22
Word2Vec+RL	-48	92	0.00
TrackVLA	122	312	0.20
GPT-4o	18	186	0.08
<b>Ours</b>	<b>234</b>	<b>435</b>	<b>0.82</b>

**Adaption to dynamic unseen target switches (Q3).** We further evaluate the ability of baseline methods to handle *dynamic target switching* when unseen target appear in the environment. Specifically, four animals (cow, dog, leopard, horse) were introduced in the FlexibleRoom, and whenever a new animal entered the view, we call the corresponding target-switching instruction (Appendix Table 10). This setting simultaneously tests both instruction comprehension and cross-category generalization.

Table 4: Real-world evaluation of UC-EVT performance on a target person walking in S-patterns for **60 seconds**, starting from three different initial distances (1.5m, 2.0m, 3.0m). We report average IoU between the current and desired bounding box positions and success rate over three trials.

Initial Distance	Avg. IoU	Success Rate
1.5m	$0.68 \pm 0.04$	0.86
2.0m	$0.78 \pm 0.05$	1.00
3.0m	$0.72 \pm 0.07$	0.98

432 As shown in Table 3, most baselines experience a sharp performance drop under target switches. Only  
 433 **HIEVT** and *Mask-PID* maintain relatively stable, with HIEVT achieving the highest success rate  
 434 (82%). Although *TrackVLA* performs well when tracking humans, its success rate drops drastically on  
 435 unseen animal categories, reflecting weak cross-category generalization. These results highlight the  
 436 difficulty of UC-EVT and the effectiveness of HIEVT in handling dynamic, multi-target scenarios.  
 437

#### 438 4.4 ABLATION STUDIES (Q4)

440 We conduct ablation studies (Table 5) to verify each component’s contribution. Our findings reveal:  
 441 1) **Goal representation:** Vector-based goals maintain reasonable episode lengths but limit precise  
 442 spatial strategy learning. CLIP-encoded text goals perform poorly due to CLIP’s limited semantic-  
 443 visual aligning capabilities. 2) **Training objectives:** Removing reward regression or IoU-based  
 444 rewards significantly decreases performance during goal transitions, demonstrating their critical role  
 445 in maintaining dynamic adaptability. 3) **LLM scaling:** While larger models (GPT-4o vs. Gemma3-  
 446 27B) generally provide better instruction-goal alignment, even smaller models (Gemma3-1B/4B)  
 447 achieve strong results, indicating our framework’s efficiency across computational constraints. 4)  
 448 **Memory-Augmented Goal Correction:** We further analyze the impact of memory buffer size, which  
 449 accumulates history trajectory observations to refine LLM-generated spatial goals. The larger buffer  
 450 size could store more diverse history trajectories. As shown in Figure 4, larger buffers consistently  
 451 improve average reward. This demonstrates that Goal Correction effectively adapts high-level goal  
 452 expectations to the target’s actual spatial morphology and dynamics, yielding more accurate and  
 453 stable tracking. The further sensitive analysis of IoU threshold selection is listed in Appendix F.2.

#### 454 4.5 RESULTS ON REAL-WORLD ENVIRONMENTS (Q5)

455 To demonstrate the practical applicability and robustness of our goal-behavior alignment framework,  
 456 we deploy the agent on a mobile wheel robot to handle real-world variability and dynamically adapt  
 457 to human instructions, the deployment detail and more video clips are available in Appendix J.

458 **Quantitative Analysis.** Except the quality analysis exhibited in Figure 3. We conducted additional  
 459 quantitative experiments in real-world settings. We evaluated tracking performance with the target  
 460 person walking in S-patterns for continuous 60 seconds from three different initial distances (1.5m,  
 461 2m, 3m). We measured IoU between the current and initial bounding box positions (target at the  
 462 desired location) across three trials per distance, shown in Table 4. For each setting, we repeated the  
 463 experiments five times to ensure robust and reliable performance metrics. These results demonstrate  
 464 that HIEVT excels in real-world robustness, generalization, and accuracy, successfully adapting to  
 465 real-world and varying initial conditions while maintaining high tracking performance.  
 466

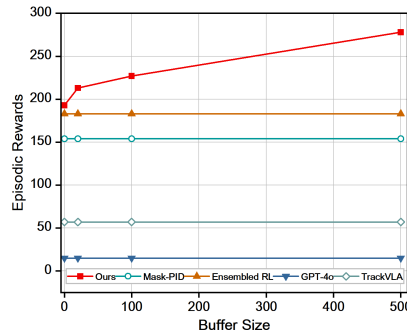
467 Table 5: Ablation study and model variant  
 468 performance comparison in FlexibleRoom  
 469 environment. Each cell shows average re-  
 470 ward/episode length/success rate.

Method	AR	EL	SR
Ours (GPT-4o)	<b>274</b>	<b>496</b>	<b>0.98</b>
Ours (Gemma3-27B)	230	492	<b>0.98</b>
Ours (Gemma3-4B)	179	484	0.94
Ours (Gemma3-1B)	144	448	0.86
w/o spatial goal(Vector)	27	487	0.46
w/o spatial goal (CLIP)	102	244	0.24
w/o reward regression	16	378	0.46
w/o IOU-based reward	-1	341	0.42

## 478 5 CONCLUSION

479 In this paper, we introduced HIEVT, a hierarchical tracking agent for User-Centric Embodied  
 480 Visual Tracking that bridges the semantic-spatial gap in human-robot interaction. Experimental  
 481 results across ten diverse environments demonstrate substantial performance advantages over existing  
 482 methods, particularly in adaptability and generalization to unseen environments. Our quality analysis  
 483 and quantitative experiment on real-world robot deployment validate that this hierarchical design  
 484 effectively balances sophisticated instruction understanding with operational efficiency, providing an  
 485 elegant and practical solution for user-guided spatial intelligence in embodied systems that scales  
 486 with minimal additional data requirements.

Figure 4: The ablation of memory buffer size.



486  
487  
**ETHICS STATEMENT**488  
489  
The authors have read and acknowledge adherence to the ICLR Code of Ethics. We address potential ethical  
considerations related to our work below:490  
491  
**Potential Applications and Societal Impact:** Our instruction-guided visual tracking method is designed for  
492 robotic applications in controlled environments such as search and rescue, elderly care assistance, and automated  
493 monitoring systems. We acknowledge that tracking technologies could potentially be misused for surveillance  
494 purposes that may infringe on privacy rights. However, our work focuses on beneficial applications and we  
encourage responsible deployment of such technologies with appropriate oversight and consent mechanisms.495  
496  
**Bias and Fairness:** The virtual environments and synthetic data used in our experiments are designed to be  
497 diverse in terms of scenes, lighting conditions, and target entities. However, we acknowledge that the simulated  
498 environments may not fully capture the diversity of real-world scenarios and populations. Future work should  
consider broader environmental and demographic diversity to ensure fair performance across different contexts.499  
500  
**Environmental Considerations:** Our experiments require computational resources for training and evaluation.  
501 We have made efforts to optimize our methods for computational efficiency and provide clear documentation to  
enable reproducible research without unnecessary resource waste.502  
503  
**Research Integrity:** All experimental results reported in this paper are obtained through rigorous experimen-  
504 tation with proper statistical analysis. We provide comprehensive implementation details and will make our  
505 code available for reproducibility. No conflicts of interest exist among the authors that could bias the research  
outcomes.506  
507  
**Data and Code Availability:** We commit to releasing our implementation code and experimental configurations  
508 to support reproducible research. The virtual environments used are publicly available through the UnrealZoo  
platform, ensuring transparency and accessibility for the research community.509  
510  
The authors believe this work contributes positively to the advancement of embodied AI research while adhering  
to ethical research practices and acknowledging potential societal implications of the developed technology.511  
512  
**REPRODUCIBILITY STATEMENT**513  
514  
To ensure the reproducibility of our research, we have made the following efforts and provide comprehensive  
515 implementation details:516  
517  
**Source Code Availability:** We provide complete source code including data collection  
518 scripts, training implementations, network architectures and virtual environment down-  
load through an anonymous repository [https://anonymous.4open.science/r/  
519 Hierarchical-Instruction-aware-Embodied-Visual-Tracking-7357/](https://anonymous.4open.science/r/Hierarchical-Instruction-aware-Embodied-Visual-Tracking-7357/). The code-  
520 base contains all necessary components to reproduce our experimental results, including hyperparameter  
521 configurations and training procedures.522  
523  
**REFERENCES**524  
525  
Peter Anderson, Qi Wu, Damien Teney, Jake Bruce, Mark Johnson, Niko Sünderhauf, Ian Reid, Stephen Gould,  
and Anton Van Den Hengel. Vision-and-language navigation: Interpreting visually-grounded navigation  
526 instructions in real environments. In *Proceedings of the IEEE conference on Computer Vision and Pattern  
527 Recognition*, pp. 3674–3683, 2018.528  
529  
Howard Chen, Alane Suhr, Dipendra Misra, Noah Snavely, and Yoav Artzi. Touchdown: Natural language  
530 navigation and spatial reasoning in visual street environments. In *Proceedings of the IEEE/CVF Conference  
on Computer Vision and Pattern Recognition*, pp. 12538–12547, 2019.531  
532  
Ho Kei Cheng, Seoung Wug Oh, Brian Price, Alexander Schwing, and Joon-Young Lee. Tracking anything  
533 with decoupled video segmentation. In *Proceedings of the IEEE/CVF International Conference on Computer  
534 Vision*, pp. 1316–1326, 2023a.535  
536  
Yangming Cheng, Liulei Li, Yuanyou Xu, Xiaodi Li, Zongxin Yang, Wenguan Wang, and Yi Yang. Segment and  
537 track anything. *arXiv preprint arXiv:2305.06558*, 2023b.538  
539  
Marius Cordts, Mohamed Omran, Sebastian Ramos, Timo Rehfeld, Markus Enzweiler, Rodrigo Benenson, Uwe  
Franke, Stefan Roth, and Bernt Schiele. The cityscapes dataset for semantic urban scene understanding. In  
*Proceedings of the IEEE conference on Computer Vision and Pattern Recognition*, pp. 3213–3223, 2016.

540 Danny Driess, Fei Xia, Mehdi SM Sajjadi, Corey Lynch, Aakanksha Chowdhery, Brian Ichter, Ayzaan Wahid,  
 541 Jonathan Tompson, Quan Vuong, Tianhe Yu, et al. Palm-e: An embodied multimodal language model. In  
 542 *International Conference on Machine Learning*, pp. 8469–8488. PMLR, 2023.

543 Guy Hoffman, Tapomayukh Bhattacharjee, and Stefanos Nikolaidis. Inferring human intent and predicting  
 544 human action in human–robot collaboration. *Annual Review of Control, Robotics, and Autonomous Systems*,  
 545 7, 2024.

546 Yunfan Jiang, Agrim Gupta, Zichen Zhang, Guanzhi Wang, Yongqiang Dou, Yanjun Chen, Li Fei-Fei, Anima  
 547 Anandkumar, Yuke Zhu, and Linxi Fan. Vima: General robot manipulation with multimodal prompts. *arXiv*  
 548 preprint arXiv:2210.03094, 2(3):6, 2022.

549 Moo Jin Kim, Karl Pertsch, Siddharth Karamcheti, Ted Xiao, Ashwin Balakrishna, Suraj Nair, Rafael Rafailov,  
 550 Ethan P Foster, Pannag R Sanketi, Quan Vuong, Thomas Kollar, Benjamin Burchfiel, Russ Tedrake, Dorsa  
 551 Sadigh, Sergey Levine, Percy Liang, and Chelsea Finn. OpenVLA: An open-source vision-language-action  
 552 model. In *8th Annual Conference on Robot Learning*, 2024. URL <https://openreview.net/forum?id=ZMnD6QZAE6>.

553 Aviral Kumar, Aurick Zhou, George Tucker, and Sergey Levine. Conservative q-learning for offline reinforcement  
 554 learning. *Advances in Neural Information Processing Systems*, 33:1179–1191, 2020.

555 Laura Leal-Taixé, Anton Milan, Ian Reid, Stefan Roth, and Konrad Schindler. Motchallenge 2015: Towards a  
 556 benchmark for multi-target tracking. *arXiv preprint arXiv:1504.01942*, 2015.

557 Mengqi Lei, Siqi Li, Yihong Wu, Han Hu, You Zhou, Xinhua Zheng, Guiguang Ding, Shaoyi Du, Zongze Wu,  
 558 and Yue Gao. Yolov13: Real-time object detection with hypergraph-enhanced adaptive visual perception.  
 559 *arXiv preprint arXiv:2506.17733*, 2025.

560 Shuo Li, Kirsty Milligan, Phil Blythe, Yanghanzi Zhang, Simon Edwards, Nic Palmarini, Lynne Corner, Yanjie  
 561 Ji, Fan Zhang, and Anil Namdeo. Exploring the role of human-following robots in supporting the mobility  
 562 and wellbeing of older people. *Scientific reports*, 13(1):6512, 2023.

563 Shilong Liu, Zhaoyang Zeng, Tianhe Ren, Feng Li, Hao Zhang, Jie Yang, Chunyuan Li, Jianwei Yang, Hang  
 564 Su, Jun Zhu, et al. Grounding dino: Marrying dino with grounded pre-training for open-set object detection.  
 565 *arXiv preprint arXiv:2303.05499*, 2023.

566 Wenhan Luo, Peng Sun, Fangwei Zhong, Wei Liu, Tong Zhang, and Yizhou Wang. End-to-end active object  
 567 tracking and its real-world deployment via reinforcement learning. *IEEE Transactions on Pattern Analysis  
 568 and Machine Intelligence*, 2019.

569 Xiaoxuan Ma, Stephan Paul Kaufhold, Jiajun Su, Wentao Zhu, Jack Terwilliger, Andres Meza, Yixin Zhu,  
 570 Federico Rossano, and Yizhou Wang. ChimpACT: A longitudinal dataset for understanding chimpanzee  
 571 behaviors. In *Thirty-seventh Conference on Neural Information Processing Systems Datasets and Benchmarks  
 572 Track*, 2023.

573 Tomas Mikolov, Kai Chen, Greg Corrado, and Jeffrey Dean. Efficient estimation of word representations in  
 574 vector space. *arXiv preprint arXiv:1301.3781*, 2013.

575 Matthias Müller and Vladlen Koltun. Openbot: Turning smartphones into robots. In *2021 IEEE International  
 576 Conference on Robotics and Automation (ICRA)*, pp. 9305–9311. IEEE, 2021.

577 Kelvin Olaiya, Giovanni Delnevo, Chiara Ceccarini, Chan-Tong Lam, Giovanni Pau, and Paola Salomoni.  
 578 Natural language and llms in human-robot interaction: Performance and challenges in a simulated setting. In  
 579 *2025 7th International Congress on Human-Computer Interaction, Optimization and Robotic Applications  
 580 (ICHORA)*, pp. 1–8. IEEE, 2025.

581 Sudipta Paul, Amit Roy-Chowdhury, and Anoop Cherian. Avlen: Audio-visual-language embodied navigation  
 582 in 3d environments. *Advances in Neural Information Processing Systems*, 35:6236–6249, 2022.

583 Pablo Pueyo, Juan Dendarrieta, Eduardo Montijano, Ana Cristina Murillo, and Mac Schwager. Cinempc: A fully  
 584 autonomous drone cinematography system incorporating zoom, focus, pose, and scene composition. *IEEE  
 585 Transactions on Robotics*, 40:1740–1757, 2024.

586 Xavier Puig, Eric Undersander, Andrew Szot, Mikael Dallaire Cote, Tsung-Yen Yang, Ruslan Partsey, Ruta  
 587 Desai, Alexander William Clegg, Michal Hlavac, So Yeon Min, et al. Habitat 3.0: A co-habitat for humans,  
 588 avatars and robots. *arXiv preprint arXiv:2310.13724*, 2023.

594 Weichao Qiu, Fangwei Zhong, Yi Zhang, Siyuan Qiao, Zihao Xiao, Tae Soo Kim, Yizhou Wang, and Alan Yuille.  
 595 Unrealcv: Virtual worlds for computer vision. In *Proceedings of the 2017 ACM on Multimedia Conference*,  
 596 pp. 1221–1224, 2017.

597  
 598 Nguyen Van Toan, Minh Do Hoang, Phan Bui Khoi, and Soo-Yeong Yi. The human-following strategy for  
 599 mobile robots in mixed environments. *Robotics and Autonomous Systems*, 160:104317, 2023.

600 Shaoan Wang, Jiazhao Zhang, Minghan Li, Jiahang Liu, Anqi Li, Kui Wu, Fangwei Zhong, Junzhi Yu, Zhizheng  
 601 Zhang, and He Wang. Trackvla: Embodied visual tracking in the wild. *arXiv preprint arXiv:2505.23189*,  
 602 2025.

603 Jason Wei, Xuezhi Wang, Dale Schuurmans, Maarten Bosma, Fei Xia, Ed Chi, Quoc V Le, Denny Zhou, et al.  
 604 Chain-of-thought prompting elicits reasoning in large language models. *Advances in neural information*  
 605 *processing systems*, 35:24824–24837, 2022.

606  
 607 Xinyi Wu, Haohong Wang, and Aggelos K Katsaggelos. Automatic camera movement generation with enhanced  
 608 immersion for virtual cinematography. *IEEE Transactions on Multimedia*, 2025.

609 Hanjing Ye, Jieting Zhao, Yaling Pan, Weinan Chen, Li He, and Hong Zhang. Robot person following under  
 610 partial occlusion. *arXiv preprint arXiv:2302.02121*, 2023.

611  
 612 Takashi Yoshimi, Manabu Nishiyama, Takafumi Sonoura, Hideichi Nakamoto, Seiji Tokura, Hirokazu Sato,  
 613 Fumio Ozaki, Nobuto Matsuhira, and Hiroshi Mizoguchi. Development of a person following robot with  
 614 vision based target detection. In *2006 IEEE/RSJ International Conference on Intelligent Robots and Systems*,  
 615 pp. 5286–5291. IEEE, 2006.

616 Libo Zhang, Junyuan Gao, Zhen Xiao, and Heng Fan. Animaltrack: A benchmark for multi-animal tracking in  
 617 the wild. *International Journal of Computer Vision*, 131(2):496–513, 2023.

618  
 619 Fangwei Zhong, Weichao Qiu, Tingyun Yan, Alan Yuille, and Yizhou Wang. Gym-unrealcv: Realistic virtual  
 620 worlds for visual reinforcement learning. Web Page, 2017. URL <https://github.com/unrealcv/gym-unrealcv>.

621  
 622 Fangwei Zhong, Peng Sun, Wenhan Luo, Tingyun Yan, and Yizhou Wang. AD-VAT: An asymmetric dueling  
 623 mechanism for learning visual active tracking. In *International Conference on Learning Representations*,  
 624 2019a. URL <https://openreview.net/forum?id=HkgYmhR9KX>.

625 Fangwei Zhong, Peng Sun, Wenhan Luo, Tingyun Yan, and Yizhou Wang. Ad-vat+: An asymmetric dueling  
 626 mechanism for learning and understanding visual active tracking. *IEEE Transactions on Pattern Analysis and*  
 627 *Machine Intelligence*, 43(5):1467–1482, 2019b.

628  
 629 Fangwei Zhong, Peng Sun, Wenhan Luo, Tingyun Yan, and Yizhou Wang. Towards distraction-robust active  
 630 visual tracking. In *International Conference on Machine Learning*, pp. 12782–12792. PMLR, 2021.

631  
 632 Fangwei Zhong, Xiao Bi, Yudi Zhang, Wei Zhang, and Yizhou Wang. Rspt: reconstruct surroundings and  
 633 predict trajectory for generalizable active object tracking. In *Proceedings of the AAAI Conference on Artificial*  
 634 *Intelligence*, volume 37, pp. 3705–3714, 2023.

635  
 636 Fangwei Zhong, Kui Wu, Hai Ci, Churan Wang, and Hao Chen. Empowering embodied visual tracking with  
 637 visual foundation models and offline rl. In *European Conference on Computer Vision*, pp. 139–155. Springer,  
 2024.

638  
 639 Fangwei Zhong, Kui Wu, Churan Wang, Hao Chen, Hai Ci, Zhoujun Li, and Yizhou Wang. Unrealzoo: Enriching  
 640 photo-realistic virtual worlds for embodied ai. In *Proceedings of the IEEE/CVF International Conference on*  
*Computer Vision (ICCV)*, 2025. URL <https://openreview.net/forum?id=vQ1y086Kn2>.

641  
 642 Qinzhong Zhou, Sunli Chen, Yisong Wang, Haozhe Xu, Weihua Du, Hongxin Zhang, Yilun Du, Joshua B.  
 643 Tenenbaum, and Chuang Gan. HAZARD challenge: Embodied decision making in dynamically changing  
 644 environments. In *The Twelfth International Conference on Learning Representations*, 2024. URL <https://openreview.net/forum?id=n6mLhaBahJ>.

645  
 646 Jie Zuo, Jun Huo, Xiling Xiao, Yanzhao Zhang, and Jian Huang. Human-robot coordination control for sit-to-  
 647 stand assistance in hemiparetic patients with supernumerary robotic leg. *IEEE Transactions on Automation*  
*Science and Engineering*, 2025.

648 **A APPENDIX**  
649650 **B USAGE OF LARGE LANGUAGE MODELS (LLMs)**  
651652 Large Language Models were used in this work solely as a writing assistance tool. Specifically, we utilized  
653 LLMs for: **Language polishing and refinement**: Improving sentence structure, grammar, and overall readability  
654 of the manuscript.655 **Important clarifications:**  
656657 

- 658 LLMs were **not** involved in research ideation, methodology design, experimental design, or result  
interpretation.
- 659 All technical contributions, algorithmic innovations, and scientific insights are entirely the work of the  
human authors.
- 660 LLMs did not generate any substantial content, figures, tables, or technical descriptions.
- 661 The research direction, experimental methodology, and all conclusions were independently developed  
by the authors.
- 662 LLM assistance was limited to linguistic improvements of already-written content, with all technical  
and scientific content remaining unchanged.

  
663664 The role of LLMs in this work was purely editorial and did not contribute to the research contributions or  
665 scientific merit of the paper.666 **C PRELIMINARIES**  
667668 **Problem Definition.** User-Centric Embodied Visual Tracking (UC-EVT) starts with an initial user instruction  
669 and a target. The tracker then attempts to track the target immediately by following the user’s instruction. The  
670 main components of this problem are outlined as follows:671 

- 672 **User Instruction.** The user initially provides an instruction  $\mathcal{I}_0$ , which serves as the starting command for the  
tracking agent. At any subsequent time step  $t$ , the user can issue a new instruction  $\mathcal{I}_t$  to update the agent’s  
behavior.
- 673 **Tracking State.** The tracking agent’s state at time  $t$ , denoted as  $s_t$ , is represented by the relative distance  $\rho_t$   
674 and the relative angle  $\theta_t$  with respect to the target. Specifically, the tracking state is given as:  $\mathcal{S}_t = (\rho_t, \theta_t)$ .
- 675 **Agent Action.** At each time step  $t$ , the tracking agent executes an action  $a_t$  to adjust its position and orientation  
676 in order to minimize the discrepancy between the current tracking state and the user’s instruction.
- 677 **Environment Transferring.** To ensure applicability to real-world scenarios, the tracker should be tested  
678 in unseen environments. This setup is designed to test the generalization and transferability of the tracking  
679 system.

  
680681 **Objective Function.** The goal of UC-EVT is to minimize the discrepancy between the user instruction  $\mathcal{I}_t$   
682 and the tracking state  $s_t$  throughout the entire tracking period  $T$ . This discrepancy is measured using a distance  
683 function  $\mathcal{D}(\mathcal{I}_t, s_t)$ . The objective function is defined as  $\min \sum_{t=1}^T \mathcal{D}(\mathcal{I}_t, s_t)$ , where  $\mathcal{D}(\mathcal{I}_t, s_t)$  quantifies the  
684 difference between the user instruction  $\mathcal{I}_t$  and the tracking state  $s_t$  at each time step  $t$ . The objective aims to  
685 ensure that the tracking agent follows the user’s instructions as closely as possible over the entire tracking period  
686 (episode).687 To better difference UC-EVT task with previous EVT task, we present a clearer comparison, shown in Table 6.  
688689 **Table 6: Comparison between Traditional EVT and User-Centric EVT**  
690691 

692 <b>Aspect</b>	693 <b>Traditional EVT</b>	694 <b>UC-EVT (Ours)</b>
695 User Control	696 System restart for new target	697 Natural language during tracking
698 Tracking Distance	699 Static	700 Changeable
701 Viewing Angle	702 Static	703 Changeable
	704 Interaction Frequency	705 Only at initialization
		706 Continuous

## 702 D VIRTUAL ENVIRONMENT

704 Our experiments were conducted across 10 diverse virtual environments built using Unreal Engine and integrating  
 705 UnrealCV (Qiu et al., 2017) for programmatic control. Specifically, we extend from the previous public EVT  
 706 benchmark Gym-UnrealCV (Zhong et al., 2024), adopting the original FlexibleRomm (SimpleRoom in EVT  
 707 benchmark) for training, ParkingLot as an unseen environment for testing. The remaining 8 unseen environments  
 708 serve as an enlargement of the original EVT benchmark environments, which increase the challenge in terms of  
 709 visual dynamic realism and context complexity. The enlarged environments are developed based on UnrealZoo  
 710 (Zhong et al., 2025), aiming to evaluate different aspects of instruction-aware tracking under various challenging  
 711 conditions. Environment binary could be downloaded from <https://modelscope.cn/datasets/UnrealZoo/UnrealZoo-UE4>, and code are available in <https://anonymous.4open.science/r/Hierarchical-Instruction-aware-Embodied-Visual-Tracking-7357/>. Though some  
 712 recent simulators provide human following functionalities, such as Habitat (Puig et al., 2023), we find their  
 713 environmental diversity and task configuration are limited, incapable of comprehensively evaluating the UC-EVT  
 714 task, here we compare them in Table 7, demonstrating the necessity of the benchmark extension.

716 Table 7: Comparison of UC-EVT with Related Benchmarks

718 Aspect	719 UC-EVT	720 Habitat 3.0	721 Gym-UnrealCV
720 Environment	721 indoor+outdoor	722 indoor	723 indoor+outdoor
721 Humanoid	722 ✓	723 ✓	724 ✓
722 Unseen Targets	723 ✓	724 ✗	725 ✓
723 Speed Variant	724 ✓	725 ✗	726 ✗
724 Distance config.	725 ✓	726 ✗	727 ✗
725 Angle config.	726 ✓	727 ✗	728 ✗
726 Target select.	727 ✓ Anytime	728 ✗	729 ✓ System init
727 Goal Spec.	728 ✓ Natural language	729 ✗	730 ✗
728 Dynamic switch goal	729 ✓	730 ✗	

## 729 D.1 TRAINING ENVIRONMENT

731 **FlexibleRoom:** This environment, adopted from previous work Zhong et al. (2023; 2021), serves as our primary  
 732 training venue. It features an adaptable indoor space with programmable lighting conditions, furniture layouts,  
 733 and target navigation patterns. The environment’s built-in navigation system enables automatic generation of  
 734 diverse trajectories through randomly sampled destinations, which is particularly valuable for data collection in  
 735 goal-conditioned reinforcement learning. We extended this environment with customizable appearance factors  
 736 like texture, lighting, and furniture placement to enhance training diversity and reduce overfitting. The modular  
 737 design allows us to systematically control visual complexity while maintaining consistency in the underlying  
 738 spatial relationships.

## 739 D.2 TESTING ENVIRONMENT

741 **Suburb:** A meticulously designed suburban neighborhood featuring irregular terrain, diverse vegetation, and  
 742 dynamic obstacles that simulate pedestrian and vehicular movement. This environment tests the agent’s ability to  
 743 maintain tracking across changing elevation, lighting conditions, and partial occlusions from trees and structures.  
 744 The open spaces combined with clustered obstacles create complex tracking scenarios with variable target  
 745 visibility.

746 **Supermarket:** An indoor retail environment with intricate item shelves, static displays, and narrow aisles that  
 747 closely mimic real-world shopping scenarios. The dense arrangement of objects creates numerous occlusion  
 748 challenges and confined spaces for navigation. This environment evaluates the system’s performance in crowded  
 749 indoor settings where the target frequently disappears behind shelves and reappears elsewhere.

750 **Parking Lot:** An outdoor environment featuring multiple parked vehicles under dim lighting conditions. The  
 751 uniform structure combined with low visibility areas and complex shadows tests the agent’s ability to discriminate  
 752 targets in visually challenging scenes. The environment transitions between open areas and confined spaces  
 753 between vehicles, requiring adaptive tracking strategies.

754 **Old Factory:** A deteriorated industrial setting characterized by numerous steel pillars, scattered wooden crates,  
 755 and uneven lighting. The environment features high ceilings with exposed structural elements and complex  
 756 shadows that create challenging visual conditions. The combination of open factory floor areas and cluttered  
 757 storage zones tests the agent’s ability to track across rapidly changing visual contexts.



Figure 5: The examples of virtual and real-world environments used in our experiments. The FlexibleRoom environment is used for training data collection, featuring diverse augmentable factor. the nine photo-realistic environments in the middle are used for quantitative evaluation, we also deploy our proposed method on three real-world scenarios to validate the effectiveness and transferability.

**Container Yard:** A dynamic logistics environment featuring stacked shipping containers under changing lighting conditions. The geometric regularity of the containers combined with dramatic lighting variations creates challenging perception scenarios. The environment features narrow corridors between container stacks that frequently occlude targets, testing the system’s ability to predict movement through temporary visual obstruction.

**Desert Ruins:** An archaeological site set in harsh desert lighting conditions with scattered walls and pillars creating a complex spatial layout. The environment combines open areas with confined passages and features extreme lighting contrasts between shadow and direct sunlight. This tests the agent’s robustness to challenging lighting conditions and irregular spatial structures.

**Brass Gardens:** A palace-style architectural complex featuring narrow corridors and multi-level platforms connected by staircases. This environment uniquely tests non-planar tracking capabilities, as targets frequently change elevation while moving through the environment. The ornate architectural elements and varying ceiling heights create complex spatial reasoning challenges for maintaining consistent tracking.

**Old Town:** A European-style hillside village with interconnected indoor and outdoor spaces linked by narrow, undulating stairways. This environment combines both open plazas and confined interior spaces, requiring frequent adaptation to changing spatial contexts. The irregular layout with multiple elevation changes tests the agent’s ability to maintain tracking continuity across diverse architectural spaces.

**Roof City:** A rooftop cityscape featuring protruding air ducts, walkways, and scattered debris that create a maze-like environment. The constrained navigation paths combined with varying elevation levels test the agent’s ability to predict movement in spatially restricted areas. The urban setting also introduces complex background textures and challenging lighting conditions from reflective surfaces.

## E LOW-LEVEL POLICY

### E.1 GOAL RANDOMIZATION AND DATA COLLECTION

In our experiment setting, the tracking goal’s relative spatial position is constrained within the range of  $\rho^* \in (200, 600)$  and  $\theta^* \in (-25^\circ, 25^\circ)$ . We uniformly sample tracking goals from this range, resulting in an offline dataset of **1,750,000** steps used to train our proposed method. In this section, we introduce the details of the data collection process, including player initialization, and state-based PID controller with noise perturbation for tracker and trajectory generation.



Figure 6: 18 humanoid models are used in data collection and evaluation.

## E.2 PLAYER INITIALIZATION

We use 18 humanoid models as targets and trackers, as shown in Figure 6. At the beginning of each episode, we randomly sample their appearance from the 18 humanoid models, and the target player will be randomly placed in the tracker's visible region.

## E.3 STATE-BASED PID CONTROLLER WITH MULTI-LEVEL PERTURBATION

We first use PID controllers to enable the agent to follow a target object, maintaining a specific distance and relative angle (e.g., 3 meters directly in front of the agent). The process is as follows:

- Setpoints: Define the desired distance and angle as the setpoints for the PID controller (e.g., 3 meters for distance and 0 degrees for angle).
- Process Variables: Measure the actual distance and angle between the agent and the target object using the grounded state data accessible via the UnrealCV API. These measurements serve as the process variables for the PID controller.
- Error Calculation: Calculate the error between the setpoints and the process variables, which will be used as inputs for the PID controller.
- Control Output: Apply the PID equation to generate the control output, determining the agent's speed and direction:

$$u(t) = K_p e(t) + K_i \int_0^t e(\tau) d\tau + K_d \frac{de(t)}{dt} \quad (6)$$

where  $u(t)$  is the control output,  $e(t)$  is the error,  $K_p$ ,  $K_i$ , and  $K_d$  are the proportional, integral, and derivative gains, respectively.

- Fine-tune the PID gains to achieve optimal controller performance. For instance, increasing  $K_p$  will enhance the agent's responsiveness to errors but may introduce overshoot or oscillations. Raising  $K_i$  helps minimize steady-state error but can lead to integral windup or slower response. Boosting  $K_d$  reduces overshoot and dampens oscillations but may also amplify noise or cause derivative kick. If the control output exceeds the defined action space limits, it is clipped. The tuned gains are detailed in Table 8.

Table 8: The parameters we used in the state-based PID controller.

Controller	$K_p$	$K_i$	$K_d$
Speed	5	0.1	0.05
Angle	1	0.01	0

Then, we introduce noise perturbation to the PID output, causing the agent to alternately deviate from and recover towards the desired distance and angle. This set-up aims to collect trajectories with diverse step rewards, alleviating the overestimation problem during offline training. We set a threshold  $p = 0.15$ , and if the probability value at time  $t$  is greater than  $p$ , which is  $P(t) > p$ , the agent takes a random action from the action space and

864 continues for  $L$  steps. We also adopt a random strategy to set the step length  $L$ , with an upper limit of 4. After  
 865 the random actions of the agent end, we use a random function to determine the duration of the next random  
 866 action  $L$ . Here, we set the upper limit to 4 because we found that the number of times the agent failed in a round  
 867 significantly increased beyond 4. Therefore, we empirically set the upper limit of the random step length to 4.  
 868

## 869 F HIGH-LEVEL SEMANTIC-SPATIAL GOAL ALIGNER

870  
 871 During training phase, we implement goal randomization within a continuous space, within the range of  
 872  $\rho^* \in (200, 600)$  and  $\theta^* \in (-25^\circ, 25^\circ)$ . However, due to computational constraints, it is impractical to  
 873 evaluate all points within this continuous space. Therefore, we constructed an instruction list through a two-step  
 874 process: first, we defined a sequence of spatial position transitions; then, we generated corresponding language  
 875 instructions for each transition.  
 876

### 877 F.1 INSTRUCTIONS GENERATION

878 To fairly and accurately evaluate our method’s ability to align with human-like real world instructions, we  
 879 generated a list of sequential text instructions by first defining various spatial objective transitions (right column  
 880 in Table 10), then we generate a corresponding natural language instruction by leveraging GPT-4o API (left  
 881 column in Table 10). These instructions, as shown in Table 10, are designed to reflect both absolute and relative  
 882 position changes, as well as some ambiguous representation and target-switching behaviors. The instructions are  
 883 organized into two main categories: sequential instructions and target-switching instructions:  
 884

**885 Sequential instructions** are designed to evaluate the model’s ability to dynamically understand and align with a  
 886 sequence of instructions over time. These instructions require the agent to follow a series of spatial objectives,  
 887 each dependent on the previous one. By evaluating the agent’s performance with sequential commands, we test  
 888 the system’s capacity to adapt its behavior as the instruction set evolves, ensuring that the model can consistently  
 889 track and follow a set of changing goals.  
 890

**891 Target-switching instructions**, on the other hand, are aimed at evaluating the model’s dynamic generalization  
 892 ability to different target categories under changing conditions. These instructions ask the agent to switch focus  
 893 from one target (e.g., “the person”) to another (e.g., “the beagle”), while maintaining consistent tracking and  
 894 navigation behavior.  
 895

**896 To balance natural language variation with consistent evaluation metrics**, we manually map these instructions  
 897 to the expected absolute or relative spatial transitions for each instruction. This predefined mapping serves as a  
 898 benchmark, allowing for objective comparison between the agent’s actions and the desired user intent.  
 899

### 900 F.2 SENSITIVITY EXPERIMENT ON IOU THRESHOLD SELECTION

901 The threshold of 0.5 in the equation 3 is empirically set. The IoU threshold aims to correct unreasonable goals  
 902 while tolerating tiny deviations. We conduct additional sensitivity experiments, shown in Table 9. Performance  
 903 remains robust across IoU thresholds [0.4, 0.7], with optimal results at 0.5 (AR=278, SR=1.0). Thresholds below  
 904 0.4 compromise tracking precision, while values above 0.7 overly penalize minor deviations. We adopt 0.5 to  
 905 balance accuracy and robustness.  
 906

907 Table 9: IoU Threshold Sensitivity Analysis

908 <b>IoU Threshold</b>	909 <b>AR</b>	910 <b>EL</b>	911 <b>SR</b>
912 0.3	913 246	914 481	915 0.92
916 0.4	917 259	918 494	919 0.98
920 0.5	921 278	922 500	923 1.0
924 0.6	925 270	926 500	927 1.0
928 0.7	929 271	930 489	931 0.96

918 Table 10: Examples of instruction pools, including sequential instructions and target switch instructions,  
 919 along with the corresponding spatial goal transitions.

921 <b>Instruction</b>	922 <b>Corresponding Spatial Goal Transition</b>
<i>Sequential Instructions</i>	
923 Keep the person in the close center, move slightly 924 to the left, increase the distance, keep the person 925 at the far center.	target $\leftarrow$ person, $(200, 0^\circ) \rightarrow (200, -20^\circ) \rightarrow$ $(350, -20^\circ) \rightarrow (450, 0^\circ)$
926 Maintain the person on the right, bring the person 927 closer, stay roughly near the center, keep the person 928 aligned to the left.	target $\leftarrow$ person, $(350, 20^\circ) \rightarrow (200, 20^\circ) \rightarrow$ $(350, 0^\circ) \rightarrow (350, -20^\circ)$
929 Keep the person in the far-away center, shift a bit 930 to the right, make sure it is not too far away, keep 931 the person in the close center.	target $\leftarrow$ person, $(450, 0^\circ) \rightarrow (450, 20^\circ) \rightarrow (\rho^* \leq$ $350, 20^\circ) \rightarrow (200, 0^\circ)$
932 Position the person on the left, move the person 933 closer, stay closer but still on the left side, keep the 934 person in the center at close range.	target $\leftarrow$ person, $(350, -20^\circ) \rightarrow (200, -20^\circ) \rightarrow$ $(\rho^* \leq 250, -20^\circ) \rightarrow (200, 0^\circ)$
935 Keep the person directly ahead, move slightly to 936 the right, increase the distance, keep the person far 937 on the right.	target $\leftarrow$ person, $(350, 0^\circ) \rightarrow (350, 20^\circ) \rightarrow$ $(450, 20^\circ) \rightarrow (450, 20^\circ)$
938 Ensure the person is on the left, reduce the distance, 939 stay roughly near the center, maintain the person 940 at medium range in front.	target $\leftarrow$ person, $(350, -20^\circ) \rightarrow (200, -20^\circ) \rightarrow$ $(350, 0^\circ) \rightarrow (350, 0^\circ)$
941 Keep the person near the center, step back slightly, 942 move slightly to the left, keep the person far on the 943 left side.	target $\leftarrow$ person, $(200, 0^\circ) \rightarrow (350, 0^\circ) \rightarrow$ $(350, -20^\circ) \rightarrow (450, -20^\circ)$
944 Keep the person in the close right, increase the 945 distance, shift slightly to the left, keep the person 946 at the far center.	target $\leftarrow$ person, $(200, 20^\circ) \rightarrow (350, 20^\circ) \rightarrow$ $(350, 0^\circ) \rightarrow (450, 0^\circ)$
947 Position the person at medium distance in the 948 center, move slightly to the right, reduce the distance, 949 keep the person close in the center.	target $\leftarrow$ person, $(350, 0^\circ) \rightarrow (350, 20^\circ) \rightarrow$ $(200, 20^\circ) \rightarrow (200, 0^\circ)$
950 Keep the person in the far left, move closer, stay 951 roughly in front, keep the person at medium range 952 in the center.	target $\leftarrow$ person, $(450, -20^\circ) \rightarrow (350, -20^\circ) \rightarrow$ $(350, 0^\circ) \rightarrow (350, 0^\circ)$
953 Start with the person at close right, gradually in- 954 crease distance, move to center alignment, then 955 position far to the left.	target $\leftarrow$ person, $(200, 20^\circ) \rightarrow (350, 20^\circ) \rightarrow$ $(400, 0^\circ) \rightarrow (450, -20^\circ)$
956 Position the person at medium right, increase dis- 957 tance while maintaining angle, shift to left align- 958 ment, bring closer to medium left.	target $\leftarrow$ person, $(350, 20^\circ) \rightarrow (450, 20^\circ) \rightarrow$ $(450, -20^\circ) \rightarrow (350, -20^\circ)$
959 Keep the person close center, move to close right, 960 step back to medium distance, finally position far 961 right.	target $\leftarrow$ person, $(200, 0^\circ) \rightarrow (200, 20^\circ) \rightarrow$ $(350, 20^\circ) \rightarrow (450, 20^\circ)$
962 Maintain person at close left, step back gradually, 963 center the alignment, continue stepping back to far 964 center.	target $\leftarrow$ person, $(200, -20^\circ) \rightarrow (350, -20^\circ) \rightarrow$ $(350, 0^\circ) \rightarrow (450, 0^\circ)$
965 Position person at medium center, shift to medium 966 left, increase distance to far left, then center while 967 maintaining far distance.	target $\leftarrow$ person, $(350, 0^\circ) \rightarrow (350, -20^\circ) \rightarrow$ $(450, -20^\circ) \rightarrow (450, 0^\circ)$
968 Keep person far right, bring significantly closer 969 to close right, shift toward center, maintain close 970 center position.	target $\leftarrow$ person, $(450, 20^\circ) \rightarrow (200, 20^\circ) \rightarrow$ $(200, 10^\circ) \rightarrow (200, 0^\circ)$
971 Start with person close right, move to medium 972 right, shift to medium center, then extend to far 973 center.	target $\leftarrow$ person, $(200, 20^\circ) \rightarrow (350, 20^\circ) \rightarrow$ $(350, 0^\circ) \rightarrow (450, 0^\circ)$
974 Position person at far left, bring to medium left, 975 center the alignment, then move closer to close 976 center.	target $\leftarrow$ person, $(450, -20^\circ) \rightarrow (350, -20^\circ) \rightarrow$ $(350, 0^\circ) \rightarrow (200, 0^\circ)$
977 Keep person at medium left, extend to far left, shift 978 toward center while maintaining distance, bring 979 closer to medium center.	target $\leftarrow$ person, $(350, -20^\circ) \rightarrow (450, -20^\circ) \rightarrow$ $(450, 0^\circ) \rightarrow (350, 0^\circ)$

Continued on next page

Table 10 – continued from previous page	
Instruction	Corresponding Spatial Goal Transition
Start close center, move to close left, extend distance to medium left, further extend to far left.	target $\leftarrow$ person, $(200, 0^\circ) \rightarrow (200, -20^\circ) \rightarrow (350, -20^\circ) \rightarrow (450, -20^\circ)$
Position person far right, shift slightly toward center, bring much closer, maintain close center-right.	target $\leftarrow$ person, $(450, 20^\circ) \rightarrow (450, 10^\circ) \rightarrow (250, 10^\circ) \rightarrow (200, 15^\circ)$
Keep person close left, extend to medium left, shift to medium right, bring closer to close right.	target $\leftarrow$ person, $(200, -20^\circ) \rightarrow (350, -20^\circ) \rightarrow (350, 20^\circ) \rightarrow (200, 20^\circ)$
Start medium center, shift to medium right, extend to far right, center while maintaining far distance.	target $\leftarrow$ person, $(350, 0^\circ) \rightarrow (350, 20^\circ) \rightarrow (450, 20^\circ) \rightarrow (450, 0^\circ)$
<i>Target-Switching Instructions</i>	
“Switch to tracking the beagle, keep it on the right.”	target $\leftarrow$ dog, $(350, 20^\circ)$
“Track the dog with a far distance.”	target $\leftarrow$ dog, $(450, 0^\circ)$
“Follow the beagle from the left side.”	target $\leftarrow$ dog, $(350, 20^\circ)$
“Follow the cow now, keep it on the left.”	target $\leftarrow$ cow, $(350, -20^\circ)$
“Track the cow at a safe distance.”	target $\leftarrow$ cow, $(450, 0^\circ)$
“Keep your eye on the cow”	target $\leftarrow$ cow, $(350, 0^\circ)$
“Tracking the leopard, keep it on a far distance.”	target $\leftarrow$ leopard, $(450, 0^\circ)$
“Follow the leopard from the left side, keep a safe distance.”	target $\leftarrow$ leopard, $(450, 20^\circ)$
“Stop following the person, track the horse.”	target $\leftarrow$ horse, $(350, 0^\circ)$
“Look at the horse, follow it.”	target $\leftarrow$ horse, $(350, 0^\circ)$
“keep following the horse from right side.”	target $\leftarrow$ horse, $(350, -20^\circ)$
“Switch back to the person at close range.”	target $\leftarrow$ person, $(200, 0^\circ)$

## G IMPLEMENTATION DETAILS

In this section, we detail the implementation of our basic setup, baseline methods, and proposed policy network structures.

Table 11: The fine-tuned parameter for Bbox-based PID Controller.

Controller	$K_p$	$K_i$	$K_d$
Speed	0.2	0.01	0.03
Angle	0.05	0.01	0.1

### G.1 BASIC SETTING

In our experiments, we utilize a continuous action space for agent movement control. The action space comprises two variables: the angular velocity, ranging from  $(-30^\circ/s, 30^\circ/s)$  and the linear velocity, ranging from  $(-1 m/s, 1 m/s)$ . We train our models using the Adam optimizer with a learning rate of  $3e-5$  and a batch size of 128.

### G.2 BASELINE METHODS

**Mask-PID:** A traditional two-stage tracking paradigm. A PID controller aligns the mask with the instructed spatial goal, while a simple regex-based parser maps natural language directives to predefined goals. To facilitate the influence of different vision models Lei et al. (2025); Liu et al. (2023); Cheng et al. (2023b), focusing on the limitation of traditional tracking paradigm, we leverage the virtual environment built on UnrealEngine and the unrealcv api Qiu et al. (2017) to generate the ground truth target’s mask, using predefined bounding box images as the goal representation, adjusting the agent’s actions to maximize the intersection-over-union (IoU) with the target mask. We implemented two PID controllers to jointly control the agent’s movement: one for linear velocity and one for angular velocity. For linear velocity ( $V_{linear}$ ), we use the areas of the target bounding box mask  $A_{goal}$  detected from state  $s$ , and goal bounding box masks  $A_{goal}$  as input variables, the  $V_{linear}$  is calculated as:

$$V_{linear}(t) = K_p(A_{goal} - A_s(t)) + K_i \int_0^t (A_{goal} - A_s(\tau)) d\tau + K_d \frac{d(A_{goal} - A_s(t))}{dt} \quad (7)$$

1026 where  $K_p$ ,  $K_i$ , and  $K_d$  are the proportional, integral, and derivative gains, respectively. The linear velocity  
 1027 is constrained within the range  $(-100, 100)$  to match the training setup. A positive  $V_{linear}$  moves the agent  
 1028 forward if  $A_s$  is smaller than  $A_{goal}$ .

1029 For angular velocity ( $V_{ang}$ ), the PID controller aims to minimize the angular deviation by computing the  
 1030 difference between the x-axis coordinates of the centers of the target mask  $x_s$  and the goal mask  $x_c$ , the  
 1031 visualization is shown in Figure 7. The control input  $V_{ang}$  is given by:  
 1032

$$V_{ang}(t) = K_p(x_c - x_s(t)) + K_i \int_0^t (x_c - x_s(\tau)) d\tau + K_d \frac{d(x_c - x_s(t))}{dt} \quad (8)$$

1033 where  $K_p$ ,  $K_i$ , and  $K_d$  are the proportional, integral, and derivative gains, respectively. The angular velocity is  
 1034 constrained within the range  $(-30, 30)$ . A positive  $V_{ang}$  results in a rightward rotation if  $x_s$  is to the right of  $x_c$ .  
 1035 The final tuned parameters are detailed in the Table 11.

1036 **Ensembled RL:** An extension of the state-of-the-art RL-based EVT model(ECCV24), where multiple policies  
 1037 are trained under different spatial goals  $(\rho^*, \theta^*)$ , and a regular expression (regex) is used during evaluation to  
 1038 select the policy that best matches the goal inferred from natural language instructions. Specifically, We trained  
 1039 four separate policy networks corresponding to four representative discrete goals:  $[g_{close}, g_{far}, g_{left}, g_{right}]$ .  
 1040 The corresponding data for these goals were extracted and filtered from the 1750000 steps offline dataset,  
 1041 providing a focused dataset for training ensemble policies. The policy network architecture is based on the  
 1042 latest state-of-the-art method for Embodied Visual Tracking (EVT) as described by Zhong et al. (2024). Dur-  
 1043 ing evaluation, we choose the corresponding policy based on the goal spatial position indicated by the instruction.  
 1044

1045 **Word2Vec+RL:** A variant of the Ensembled RL baseline where we jointly train an instruction encoder by  
 1046 applying pretrained word2vec-google-news-300 Mikolov et al. (2013) with a policy network, instead of relying  
 1047 on regex mapping. In implementation, we use the same dataset to train an end-to-end model using word2vec-  
 1048 google-news-300 Mikolov et al. (2013) for text encoding (W2V), a basic four-layer convolutional neural network  
 1049 for image encoding (CNN), with three consecutive observation frames concatenated as input, and a two-layer  
 1050 MLP for feature alignment and action prediction. We use the same Conservative-Q learning method for offline  
 1051 RL training. This approach highlights the limitations of directly combining existing NLP and neural network  
 1052 modules in an end-to-end fashion.

1053 **GPT4-o:** We leverage the multi-modal capabilities of GPT4-o to directly generate actions based on the observed  
 1054 image and the desired goal. To ensure smooth and accurate transitions, we developed a system prompt that aids  
 1055 the large model in comprehending the task and regularizes the output format, aligning it with our predefined  
 1056 action settings. This prompt serves as a guiding framework, enabling the model to produce actions that are  
 1057 coherent with the requirements of the task. Specifically, we converted the bounding box goal representation into  
 1058 text-based coordinates, and the input image was first transformed to the same text-conditioned segmentation  
 1059 mask in the paper, then detected the target's bounding box coordinates as input of LLM. Note that the system  
 1060 prompt could directly use image observation as input, but from our experience, the alignment performance is  
 1061 quite poor. The system prompt content is shown by Figure 12.

1062 **TrackVLA:** A recent the state-of-the-art VLA-based tracker Wang et al. (2025) that adapts large vision-language-  
 1063 action models to embodied visual tracking tasks. In implementation, we obtained the pre-trained model of  
 1064 TrackVLA through direct communication with the original authors via email Wang et al. (2025). This allowed  
 1065 us to directly evaluate the model in our environment using the pre-trained weights without requiring additional  
 1066 training. The only modification we made to the original TrackVLA implementation was adjusting the maximum  
 1067 speed during varying speed testing. Specifically, when testing at 2 m/s, we increased TrackVLA's speed limit to  
 1068 220 to meet the dynamic requirements (slightly higher than the target's speed for redundancy considerations).  
 1069

### 1070 G.3 POLICY NETWORK

1071 In our approach, we use convolutional neural networks (CNN) as the visual extraction module, which is followed  
 1072 by a fully connected layer and a Reward Head. The output of the reward head is used for reward regression  
 1073 during training. The output of the fully connected layer is fed into the recurrent policy network. We use a  
 1074 long-short-term memory(LSTM) network to model temporal consistency. The recurrent policy network is an  
 1075 extension of the CQL-SAC algorithm Kumar et al. (2020), where we have modified the data sampling and  
 1076 optimization processes to accommodate the LSTM network. The visual temporal features extracted by the CNN  
 1077 and LSTM are then passed to the actor and critic networks, each consisting of two fully connected layers. The  
 1078 hyperparameters and neural network structures employed in our method are detailed in Table 12 and Table 14.  
 1079

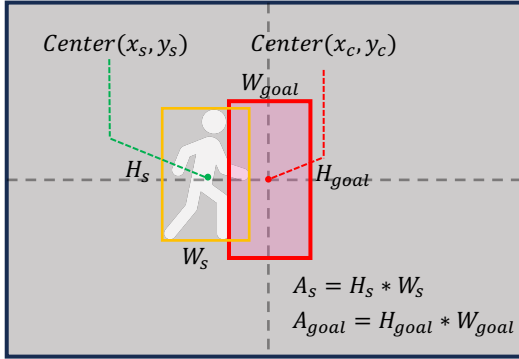


Figure 7: Illustration of the target bounding box (yellow box) and goal bounding box (red box) used in PID controller. The center of target bounding box  $Center(x_s, y_s)$  and spatial goal  $Center(x_c, y_c)$  are used to calculate horizontal deviations. The area size of target bounding box  $A_s$  and spatial goal  $A_{goal}$  are used to calculate distance deviations.

Table 12: The hyper-parameters used for offline training and the policy network.

Name	Symbol	Value
Learning Rate	$\alpha$	3e-5
Discount Factor	$\gamma$	0.99
Batch Size	-	128
LSTM update step	-	20
LSTM Input Dimension	-	256
LSTM Output Dimension	-	64
LSTM Hidden Layer size	-	1
Reward Head Input Dimension	-	256
Reward Head Output Dimension	-	1

## H LLM-BASED SEMANTIC-SPATIAL GOAL ALIGNER

In our method, we develop a hierarchical instruction parser, integrated with Large Language Models (LLM) and chain-of-thought to translate human instructions into a mid-level goal representation. We first describe our evaluation method, then visualize the evaluation result via a radar chart.

### H.1 QUALITY EVALUATION

To evaluate the effectiveness of our instruction parser and investigate the impact of different reasoning mechanisms on the accuracy of bounding box generation, we employ three different methods: GPT-4o: We use GPT-4o with a system prompt that includes both a task introduction and chain-of-thought (CoT) reasoning guidelines for evaluation. GPT-4o w/o CoT: We use GPT-4o with a system prompt containing only the task introduction for evaluation. GPT-01: We use GPT-01 with a system prompt that includes the task introduction for evaluation.

We ensure a fair evaluation by sampling 140 instructions from the instruction list in Table ??, and each instruction is paired with a corresponding spatial goal. This setup minimizes ambiguity in the textual instructions, providing a baseline for evaluating the correctness of the generated bounding boxes. The performance is assessed by the accuracy of generated bounding boxes. The accuracy is calculated as: the number of correctly generated bounding boxes divided by the total sampled instances

For each instruction, we define two categories based on the type of spatial instruction: absolute spatial positions and relative spatial position changes. The rules for evaluating bounding box correctness are as follows:

1) Instructions conveying absolute spatial positions (first 22 rows of Table 4): We use the final generated bounding box  $[x, y, w, h]$ , calculate horizontal position  $x$  and area size  $w * h$  to determine correctness.

- $(\rho^*, \theta^*) = (200, 0^\circ)$ : Valid if area size is within (0.06, 0.3) and  $x$  is within (0.4, 0.6).
- $(\rho^*, \theta^*) = (450, 0^\circ)$ : Valid if area size is within (0, 0.06) and  $x$  is within (0.4, 0.6)
- $(\rho^*, \theta^*) = (350, -20^\circ)$ : Valid if  $x$  is within (0, 0.4).

1134 Table 13: We directly map our adopted action space (continuous actions) from virtual to real. The  
 1135 second and the third columns are the value ranges of velocities in the virtual and the real robot,  
 1136 respectively.

Bound of Action	Linear	
	Virtual (cm/s)	Real (m/s)
High	100, 30	0.5, 1.0
Low	-100, -30	-0.5, -1.0
	Angular	
	Virtual (degree/s)	Real (rad/s)
High	100, 30	0.5, 1.0
Low	-100, -30	-0.5, -1.0

1146 Table 14: The neural network structure, where  $8 \times 8\text{-}16S4$  means 16 filters of size  $8 \times 8$  and stride 4,  
 1147 FC256 indicates fully connected layer with dimension 256, Reward Head 1 means the fully connected  
 1148 layer for reward regression layer with output dimension 1, and LSTM64 indicates that all the sizes in  
 1149 the LSTM unit are 64.

Module	Goal-state Aligner				Recurrent Policy		
	CNN	CNN	FC	Reward Head	LSTM	FC	FC
Parameters	$8 \times 8\text{-}16S4$	$4 \times 4\text{-}32S2$	256	1	64	2	2

1150  
 1151 •  $(\rho^*, \theta^*) = (350, 20^\circ)$ : Valid if  $x$  is within  $(0.6, 1)$ .  
 1152  
 1153 2) Instructions conveying relative spatial position change (last 20 rows of Table 4): We evaluated based on  
 1154 bounding box increments  $[\Delta x, \Delta y, \Delta w, \Delta h]$  generated by the parser.  
 1155  
 1156 •  $(\Delta\rho, \Delta\theta) = (-150, 0^\circ)$ : Valid if both  $\Delta w$  and  $\Delta h$  are positive.  
 1157 •  $(\Delta\rho, \Delta\theta) = (150, 0^\circ)$ : Valid if both  $\Delta w$  and  $\Delta h$  are negative.  
 1158 •  $(\Delta\rho, \Delta\theta) = (0, -20^\circ)$ : Valid if  $\Delta x < 0$ .  
 1159 •  $(\Delta\rho, \Delta\theta) = (0, 20^\circ)$ : Valid if  $\Delta x > 0$ .  
 1160  
 1161 The results in Figure 8 confirm that the chain-of-thought (CoT) reasoning mechanism significantly improves the  
 1162 accuracy of the bounding box generation. Compared with GPT-4o w/o CoT and GPT-o1, GPT-4o consistently  
 1163 exceeds 80%, achieving up to 100% accuracy in some cases, demonstrating its reliability in translating textual  
 1164 instructions into spatially accurate bounding boxes. We argue that CoT enhances the model’s ability to handle  
 1165 more nuanced spatial relationships. GPT-O1 performs significantly worse than GPT-4o and GPT-4o w/o CoT,  
 1166 and we believe this is largely due to the underlying reasoning mechanism. GPT-o1 employs an automatic  
 1167 decomposition reasoning approach, which decomposes tasks into smaller steps without considering the broader  
 1168 context. This lack of holistic reasoning leads to poor performance in our task, particularly when handling  
 1169 complex spatial relationships.  
 1170  
 1171

## H.2 PROMPTS

1172 We define a system prompt aiming to help the LLM understand the tracking task and introduce the Chain-of-  
 1173 thought (CoT) to enhance the LLM’s understanding ability. The detailed content of the system prompt is shown  
 1174 in Figure 11.

## I GRAPHIC USER INTERFACE

1175 To enable an intuitive visual interaction and multi-modal instruction input, we design a simple GUI for user  
 1176 input instructions while observing the environment from the tracking agent’s first-person view. Users could  
 1177 directly type text instructions and click the “send” button to update instructions. The GUI demonstration is  
 1178 shown in Figure 10.

## J REAL-WORLD DEPLOYMENT

1179 We transfer our agent into real-world scenarios to verify the practical contribution and the effectiveness of our  
 1180 proposed method. Specifically, we use **SAM-Track** Cheng et al. (2023b) to generate segmentation masks from

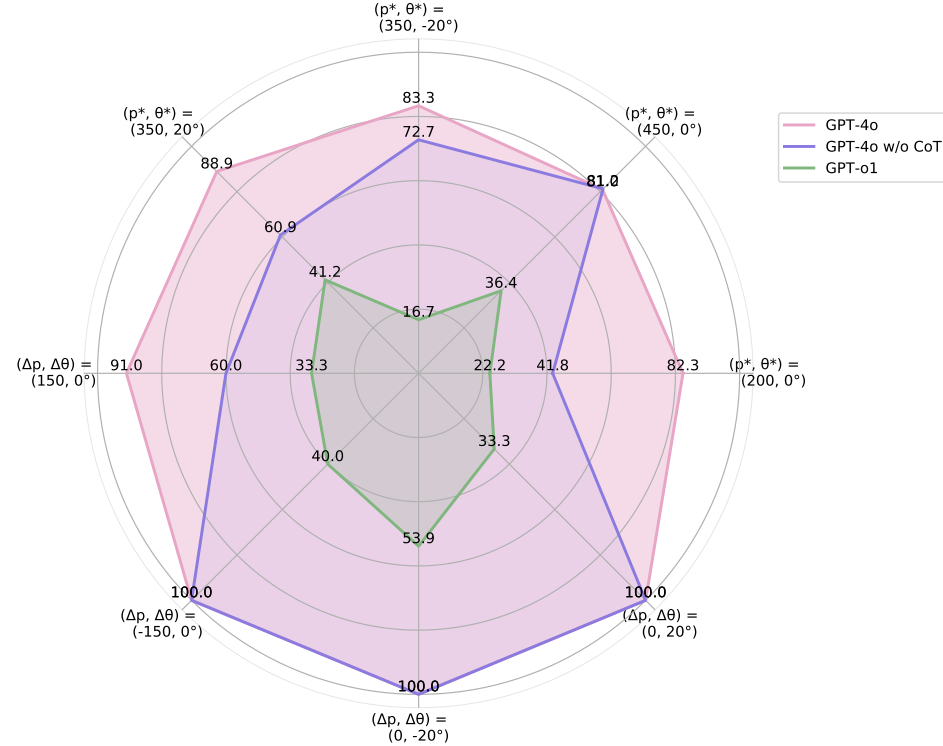
1188  
1189  
11901191 Accuracy of Generated Bounding Boxes Based on Textual  
1192 Instructions and Spatial Goals1193  
1194  
1195  
1196  
1197  
1198  
1199  
1200  
1201  
1202  
1203  
1204  
1205  
1206  
1207  
1208  
1209  
1210  
1211  
1212  
1213  
1214  
1215  
1216  
1217  
1218  
1219  
12201221  
1222

Figure 8: The accuracy of generated bounding boxes based on textual instructions and spatial goals by using GPT-4o, GPT-4o w/o CoT, and GPT-o1.

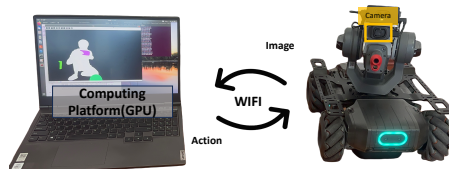
1223  
1224  
1225  
1226  
1227  
1228  
1229  
1230  
1231  
1232  
12331234  
1235  
1236  
1237

Figure 9: In this real-world deployment, the robot's onboard camera captures visual data, which is wirelessly transmitted to a laptop for real-time processing. The model on the laptop interprets the incoming images, generates appropriate action commands, and transmits them back to the robot via WiFi, enabling precise control of its movements.

1238  
1239  
1240  
1241the robot's real-time observations. Comprehensive video demonstrations of these experiments are available on our project website (<https://sites.google.com/view/hievt>).

1242  
1243  
1244  
1245  
1246  
1247  
1248  
1249  
1250  
1251



1252 Figure 10: A real-time interactive GUI snapshot. The left panel displays the tracker’s first-person  
1253 view, while the right panel shows the text-conditioned mask generated by the game engine. Users can  
1254 input instructions in the text box at the bottom or draw a bounding box (e.g., the green box in the left  
1255 image) and click the "Send" button to interact with the system.

1256  
1257

### J.1 HARDWARE SETUP

1259  
1260  
1261  
1262  
1263  
1264  
1265  
1266  
1267  
1268

To evaluate our proposed method in real-world scenarios, we use RoboMaster EP<sup>1</sup> a 4-wheeled robot manufactured by DJI, as our experimental platform (Figure 9). Equipped with an RGB camera, the RoboMaster captures images and allows direct control of linear speed and angular motion via a Python API. This advanced design ensures precise control over the robot’s movements during our experiments. To enable real-time image processing, we use a wireless LAN connection to transmit camera data to a laptop with an Nvidia RTX A3000 GPU, which acts as the computational platform to run the model and predict actions based on raw pixel images. The corresponding control signals are then sent back to the robot, completing a closed-loop control system. This seamless integration of hardware and software allows us to execute complex tasks efficiently and accurately, advancing sim-to-real experimentation. In the training phase, we use a continuous action space, which enables us to directly map the speed to robot control signals. The mapping relationship is shown in Table 13.

1269  
1270  
1271  
1272  
1273  
1274

### J.2 EXPERIMENTAL RESULTS AND OBSERVATIONS

1275  
1276  
1277  
1278  
1279  
1280  
1281  
1282  
1283  
1284  
1285  
1286

The real-world experiments were conducted to verify three key hypotheses: (1) the system can maintain robustness across diverse physical scenarios, (2) our hierarchical framework can effectively bridge the gap between language instructions and tracking behavior in real environments, and (3) the intermediate spatial goal representation provides sufficient flexibility for diverse instruction types.

1287

#### J.2.1 DYNAMIC MOVEMENT ADAPTATION

1288  
1289  
1290  
1291  
1292  
1293  
1294  
1295

The robot successfully maintained tracking while targets performed unpredictable movements including **sudden direction changes** and **varying speeds (from walking to running)**. A critical observation from these experiments was that the system’s performance directly validated our hierarchical design approach. The instruction reasoning process (running at approximately 1-2 Hz) did not interfere with the high-frequency control policy, allowing the tracking policy to operate continuously even during instruction processing. This asynchronous execution enabled the system to maintain responsive tracking while simultaneously processing complex instructions—a capability that would be impossible with end-to-end approaches like GPT-4o or OpenVLA where inference latency directly impacts control frequency. Our video demonstrations on project website clearly show this advantage in action: even when new instructions are being processed (visible through UI indicators in the videos), the robot maintains smooth, continuous tracking without pauses or hesitation. This confirms that our hierarchical framework effectively decouples semantic understanding from real-time control, enabling robust performance in dynamic real-world scenarios.

1296  
1297  
1298

#### J.2.2 SPATIAL GOAL ADAPTATION

1299  
1300  
1301  
1302  
1303  
1304  
1305  
1306  
1307  
1308  
1309  
1310  
1311  
1312  
1313  
1314  
1315  
1316  
1317  
1318  
1319  
1320  
1321  
1322  
1323  
1324  
1325  
1326  
1327  
1328  
1329  
1330  
1331  
1332  
1333  
1334  
1335  
1336  
1337  
1338  
1339  
1340  
1341  
1342  
1343  
1344  
1345  
1346  
1347  
1348  
1349  
1350  
1351  
1352  
1353  
1354  
1355  
1356  
1357  
1358  
1359  
1360  
1361  
1362  
1363  
1364  
1365  
1366  
1367  
1368  
1369  
1370  
1371  
1372  
1373  
1374  
1375  
1376  
1377  
1378  
1379  
1380  
1381  
1382  
1383  
1384  
1385  
1386  
1387  
1388  
1389  
1390  
1391  
1392  
1393  
1394  
1395  
1396  
1397  
1398  
1399  
1400  
1401  
1402  
1403  
1404  
1405  
1406  
1407  
1408  
1409  
1410  
1411  
1412  
1413  
1414  
1415  
1416  
1417  
1418  
1419  
1420  
1421  
1422  
1423  
1424  
1425  
1426  
1427  
1428  
1429  
1430  
1431  
1432  
1433  
1434  
1435  
1436  
1437  
1438  
1439  
1440  
1441  
1442  
1443  
1444  
1445  
1446  
1447  
1448  
1449  
1450  
1451  
1452  
1453  
1454  
1455  
1456  
1457  
1458  
1459  
1460  
1461  
1462  
1463  
1464  
1465  
1466  
1467  
1468  
1469  
1470  
1471  
1472  
1473  
1474  
1475  
1476  
1477  
1478  
1479  
1480  
1481  
1482  
1483  
1484  
1485  
1486  
1487  
1488  
1489  
1490  
1491  
1492  
1493  
1494  
1495  
1496  
1497  
1498  
1499  
1500  
1501  
1502  
1503  
1504  
1505  
1506  
1507  
1508  
1509  
1510  
1511  
1512  
1513  
1514  
1515  
1516  
1517  
1518  
1519  
1520  
1521  
1522  
1523  
1524  
1525  
1526  
1527  
1528  
1529  
1530  
1531  
1532  
1533  
1534  
1535  
1536  
1537  
1538  
1539  
1540  
1541  
1542  
1543  
1544  
1545  
1546  
1547  
1548  
1549  
1550  
1551  
1552  
1553  
1554  
1555  
1556  
1557  
1558  
1559  
1560  
1561  
1562  
1563  
1564  
1565  
1566  
1567  
1568  
1569  
1570  
1571  
1572  
1573  
1574  
1575  
1576  
1577  
1578  
1579  
1580  
1581  
1582  
1583  
1584  
1585  
1586  
1587  
1588  
1589  
1590  
1591  
1592  
1593  
1594  
1595  
1596  
1597  
1598  
1599  
1600  
1601  
1602  
1603  
1604  
1605  
1606  
1607  
1608  
1609  
1610  
1611  
1612  
1613  
1614  
1615  
1616  
1617  
1618  
1619  
1620  
1621  
1622  
1623  
1624  
1625  
1626  
1627  
1628  
1629  
1630  
1631  
1632  
1633  
1634  
1635  
1636  
1637  
1638  
1639  
1640  
1641  
1642  
1643  
1644  
1645  
1646  
1647  
1648  
1649  
1650  
1651  
1652  
1653  
1654  
1655  
1656  
1657  
1658  
1659  
1660  
1661  
1662  
1663  
1664  
1665  
1666  
1667  
1668  
1669  
1670  
1671  
1672  
1673  
1674  
1675  
1676  
1677  
1678  
1679  
1680  
1681  
1682  
1683  
1684  
1685  
1686  
1687  
1688  
1689  
1690  
1691  
1692  
1693  
1694  
1695  
1696  
1697  
1698  
1699  
1700  
1701  
1702  
1703  
1704  
1705  
1706  
1707  
1708  
1709  
1710  
1711  
1712  
1713  
1714  
1715  
1716  
1717  
1718  
1719  
1720  
1721  
1722  
1723  
1724  
1725  
1726  
1727  
1728  
1729  
1730  
1731  
1732  
1733  
1734  
1735  
1736  
1737  
1738  
1739  
1740  
1741  
1742  
1743  
1744  
1745  
1746  
1747  
1748  
1749  
1750  
1751  
1752  
1753  
1754  
1755  
1756  
1757  
1758  
1759  
1760  
1761  
1762  
1763  
1764  
1765  
1766  
1767  
1768  
1769  
1770  
1771  
1772  
1773  
1774  
1775  
1776  
1777  
1778  
1779  
1780  
1781  
1782  
1783  
1784  
1785  
1786  
1787  
1788  
1789  
1790  
1791  
1792  
1793  
1794  
1795  
1796  
1797  
1798  
1799  
1800  
1801  
1802  
1803  
1804  
1805  
1806  
1807  
1808  
1809  
1810  
1811  
1812  
1813  
1814  
1815  
1816  
1817  
1818  
1819  
1820  
1821  
1822  
1823  
1824  
1825  
1826  
1827  
1828  
1829  
1830  
1831  
1832  
1833  
1834  
1835  
1836  
1837  
1838  
1839  
1840  
1841  
1842  
1843  
1844  
1845  
1846  
1847  
1848  
1849  
1850  
1851  
1852  
1853  
1854  
1855  
1856  
1857  
1858  
1859  
1860  
1861  
1862  
1863  
1864  
1865  
1866  
1867  
1868  
1869  
1870  
1871  
1872  
1873  
1874  
1875  
1876  
1877  
1878  
1879  
1880  
1881  
1882  
1883  
1884  
1885  
1886  
1887  
1888  
1889  
1890  
1891  
1892  
1893  
1894  
1895  
1896  
1897  
1898  
1899  
1900  
1901  
1902  
1903  
1904  
1905  
1906  
1907  
1908  
1909  
1910  
1911  
1912  
1913  
1914  
1915  
1916  
1917  
1918  
1919  
1920  
1921  
1922  
1923  
1924  
1925  
1926  
1927  
1928  
1929  
1930  
1931  
1932  
1933  
1934  
1935  
1936  
1937  
1938  
1939  
1940  
1941  
1942  
1943  
1944  
1945  
1946  
1947  
1948  
1949  
1950  
1951  
1952  
1953  
1954  
1955  
1956  
1957  
1958  
1959  
1960  
1961  
1962  
1963  
1964  
1965  
1966  
1967  
1968  
1969  
1970  
1971  
1972  
1973  
1974  
1975  
1976  
1977  
1978  
1979  
1980  
1981  
1982  
1983  
1984  
1985  
1986  
1987  
1988  
1989  
1990  
1991  
1992  
1993  
1994  
1995  
1996  
1997  
1998  
1999  
2000  
2001  
2002  
2003  
2004  
2005  
2006  
2007  
2008  
2009  
2010  
2011  
2012  
2013  
2014  
2015  
2016  
2017  
2018  
2019  
2020  
2021  
2022  
2023  
2024  
2025  
2026  
2027  
2028  
2029  
2030  
2031  
2032  
2033  
2034  
2035  
2036  
2037  
2038  
2039  
2040  
2041  
2042  
2043  
2044  
2045  
2046  
2047  
2048  
2049  
2050  
2051  
2052  
2053  
2054  
2055  
2056  
2057  
2058  
2059  
2060  
2061  
2062  
2063  
2064  
2065  
2066  
2067  
2068  
2069  
2070  
2071  
2072  
2073  
2074  
2075  
2076  
2077  
2078  
2079  
2080  
2081  
2082  
2083  
2084  
2085  
2086  
2087  
2088  
2089  
2090  
2091  
2092  
2093  
2094  
2095  
2096  
2097  
2098  
2099  
2100  
2101  
2102  
2103  
2104  
2105  
2106  
2107  
2108  
2109  
2110  
2111  
2112  
2113  
2114  
2115  
2116  
2117  
2118  
2119  
2120  
2121  
2122  
2123  
2124  
2125  
2126  
2127  
2128  
2129  
2130  
2131  
2132  
2133  
2134  
2135  
2136  
2137  
2138  
2139  
2140  
2141  
2142  
2143  
2144  
2145  
2146  
2147  
2148  
2149  
2150  
2151  
2152  
2153  
2154  
2155  
2156  
2157  
2158  
2159  
2160  
2161  
2162  
2163  
2164  
2165  
2166  
2167  
2168  
2169  
2170  
2171  
2172  
2173  
2174  
2175  
2176  
2177  
2178  
2179  
2180  
2181  
2182  
2183  
2184  
2185  
2186  
2187  
2188  
2189  
2190  
2191  
2192  
2193  
2194  
2195  
2196  
2197  
2198  
2199  
2200  
2201  
2202  
2203  
2204  
2205  
2206  
2207  
2208  
2209  
2210  
2211  
2212  
2213  
2214  
2215  
2216  
2217  
2218  
2219  
2220  
2221  
2222  
2223  
2224  
2225  
2226  
2227  
2228  
2229  
22210  
22211  
22212  
22213  
22214  
22215  
22216  
22217  
22218  
22219  
22220  
22221  
22222  
22223  
22224  
22225  
22226  
22227  
22228  
22229  
222210  
222211  
222212  
222213  
222214  
222215  
222216  
222217  
222218  
222219  
222220  
222221  
222222  
222223  
222224  
222225  
222226  
222227  
222228  
222229  
2222210  
2222211  
2222212  
2222213  
2222214  
2222215  
2222216  
2222217  
2222218  
2222219  
2222220  
2222221  
2222222  
2222223  
2222224  
2222225  
2222226  
2222227  
2222228  
2222229  
22222210  
22222211  
22222212  
22222213  
22222214  
22222215  
22222216  
22222217  
22222218  
22222219  
22222220  
22222221  
22222222  
22222223  
22222224  
22222225  
22222226  
22222227  
22222228  
22222229  
222222210  
222222211  
222222212  
222222213  
222222214  
222222215  
222222216  
222222217  
222222218  
222222219  
222222220  
222222221  
222222222  
222222223  
222222224  
222222225  
222222226  
222222227  
222222228  
222222229  
2222222210  
2222222211  
2222222212  
2222222213  
2222222214  
2222222215  
2222222216  
2222222217  
2222222218  
2222222219  
2222222220  
2222222221  
2222222222  
2222222223  
2222222224  
2222222225  
2222222226  
2222222227  
2222222228  
2222222229  
22222222210  
22222222211  
22222222212  
22222222213  
22222222214  
22222222215  
22222222216  
22222222217  
22222222218  
22222222219  
22222222220  
22222222221  
22222222222  
22222222223  
22222222224  
22222222225  
22222222226  
22222222227  
22222222228  
22222222229  
222222222210  
222222222211  
222222222212  
222222222213  
222222222214  
222222222215  
222222222216  
222222222217  
222222222218  
222222222219  
222222222220  
222222222221  
222222222222  
222222222223  
222222222224  
222222222225  
222222222226  
222222222227  
222222222228  
222222222229  
2222222222210  
2222222222211  
2222222222212  
2222222222213  
2222222222214  
2222222222215  
2222222222216  
2222222222217  
2222222222218  
2222222222219  
2222222222220  
2222222222221  
2222222222222  
2222222222223  
2222222222224  
2222222222225  
2222222222226  
2222222222227  
2222222222228  
2222222222229  
22222222222210  
22222222222211  
22222222222212  
22222222222213  
22222222222214  
22222222222215  
22222222222216  
22222222222217  
22222222222218  
22222222222219  
22222222222220  
22222222222221  
22222222222222  
22222222222223  
22222222222224  
22222222222225  
22222222222226  
22222222222227  
22222222222228  
22222222222229  
222222222222210  
222222222222211  
222222222222212  
222222222222213  
222222222222214  
222222222222215  
222222222222216  
222222222222217  
222222222222218  
222222222222219  
222222222222220  
222222222222221  
222222222222222  
222222222222223  
222222222222224  
222222222222225  
222222222222226  
222222222222227  
222222222222228  
222222222222229  
2222222222222210  
2222222222222211  
2222222222222212  
2222222222222213  
2222222222222214  
2222222222222215  
2222222222222216  
2222222222222217  
2222222222222218  
2222222222222219  
2222222222222220  
2222222222222221  
2222222222222222  
2222222222222223  
2222222222222224  
2222222222222225  
2222222222222226  
2222222222222227  
2222222222222228  
2222222222222229  
22222222222222210  
22222222222222211  
22222222222222212  
22222222222222213  
22222222222222214  
22222222222222215  
22222222222222216  
22222222222222217  
22222222222222218  
22222222222222219  
22222222222222220  
22222222222222221  
22222222222222222  
22222222222222223  
22222222222222224  
22222222222222225  
22222222222222226  
22222222222222227  
22222222222222228  
22222222222222229  
222222222222222210  
222222222222222211  
222222222222222212  
222222222222222213  
222222222222222214  
222222222222222215  
222222222222222216  
222222222222222217  
222222222222222218  
222222222222222219  
222222222222222220  
222222222222222221  
222222222222222222  
222222222222222223  
222222222222222224  
222222222222222225  
222222222222222226  
222222222222222227  
222222222222222228  
222222222222222229  
2222222222222222210  
2222222222222222211  
2222222222222222212  
2222222222222222213  
2222222222222222214  
2222222222222222215  
2222222222222222216  
2222222222222222217  
2222222222222222218  
2222222222222222219  
2222222222222222220  
2222222222222222221  
2222222222222222222  
2222222222222222223  
2222222222222222224  
2222222222222222225  
2222222222222222226  
2222222222222222227  
2222

1296 **System Prompt**

1297

1298 **Objective:**

1299 You are an intelligent tracking agent designed to follow human instructions and  
1300 dynamically adjust your tracking goal between you and the target. Your task is  
1301 twofold:

1302 1. Identify the target category mentioned in the instruction (e.g., "person," "vehicle,"  
1303 "object").

1304 2. Understand the human instruction to determine the tracking goal. The goal is  
1305 represented as an expected bounding box position in your field of view, with the  
1306 center at  $[cx, cy]$ , width  $w$ , and height  $h$ . This will guide your tracking strategy  
1307 to align the target object with the specified bounding box. The local control  
1308 strategy will then use this expected bounding box to achieve different tracking  
1309 angles and distances based on human instruction.

1310

1311 **Representation detail:**

1312 All positions in the task should be represented as normalized bounding box coordinates  
1313 relative to the image size in the field of view with width and height (e.g.,  $[cx,$   
1314  $cy, w, h]$ ). 'cx' and 'cy' represent the center of the bounding box, and 'w' and 'h'  
1315 represent the width and height of the bounding box, respectively, all normalized  
1316 to the range  $[0, 1]$ .

1317

1318 **Task Understanding:**

1319 1. **Instruction:** A natural language command describing the desired change in the  
1320 tracking of the target (e.g., "Get closer to the person," "Move further from the  
1321 car," "Keep the dog in the center," or "Keep the object on the left").

1322 2. **Current bounding box:** The current bounding box coordinates and size of the  
1323 target in your field of view relative to the image size, normalized to  $[0, 1]$  (e.g.  
1324 .., "Target position:  $[cx, cy, w, h]$ ").

1325

1326 **Task Definition:**

1327 Your task is to:

1328 Extract the target category from the instruction (e.g., "person," "car," "dog") and  
1329 determine the expected bounding box position and size within your field of view  
1330 based on the human instruction and the current target position.

1331

1332 **This should include:**

1333 1. **Target category:** Based on the human instruction, provide the target category name  
1334 .

1335 2. **Bounding Box Increment:** Based on the human instruction, provide the change in the  
1336 bounding box. This should be represented as  $[\Delta cx, \Delta cy, \Delta w, \Delta h]$ , where  $\Delta cx$  and  
1337  $\Delta cy$  are the changes in the center coordinates, and  $\Delta w$  and  $\Delta h$  are the changes in  
1338 the width and height of the bounding box.

1339

1340 **Instructions:** Given the provided human instruction, and current position, think step by  
1341 step, decide the target category name and best bounding box increment to meet the  
1342 human's instructions.

1343

1344 **Strategy Considerations:**

1345 The given Current Position represents the current target distance and angle relative to  
1346 the tracker.

1347 The human instruction represented the demand for expected tracking distance and angle  
1348 between the target and tracker.

1349 You should consider the human instruction first, and transform the abstract instruction  
1350 into the concrete bounding box position increment.

1351 The increment value should be 20% each time with respect to the original proportion of  
1352 the target bounding box.

1353 The increment value should consider the first-person view perspective effect.

1354

1355 Provide the target category name format in "**Target category:** [target category]" and  
1356 the chain-of-thought process of the increment of bounding box position and size  
1357 end with the format "**Bounding Box Increment:** chain-of-thought process.  $[\Delta cx,$   
1358  $\Delta cy, \Delta w, \Delta h]$ " in **[output:]**

1359

1360 **Example:**

1361 Example:  
1362 [input:]

1363 Instruction: "Get closer to the person."  
1364 Current bounding box:  $[0.51, 0.57, 0.07, 0.14]$ .

1365

1366 [output:]

1367 **Target category:** [person]

1368 **Bounding Box Increment:** The current bounding box indicates it is positioned near  
1369 the center of view. If the instruction wants to get closer to the target, the  
1370 bounding box size should be larger without horizontal change and a slight  
1371 increment in vertical position, which should be increased  $\Delta w$ ,  $\Delta h$  and  $\Delta cy$ .  $[0.0,$   
1372  $0.05, 0.03, 0.17]$ .

Figure 11: System prompt used in instruction parser module.

1350  
1351  
1352  
1353  
1354  
1355  
1356  
1357  
1358  
1359

1360 **System Prompt**

1361 You are an intelligent tracking agent designed to generate discrete control actions to  
1362 control the robot to follow the target object at an expected distance and angle.  
1363  
1364 Representation detail:  
1365 Bounding box: The bounding box position and size within your field of view, represented  
1366 as [cx, cy, w, h]. 'cx' and 'cy' represent the center of the bounding box, and 'w'  
1367 and 'h' represent the width and height of the bounding box, respectively.  
1368  
1369 Control Actions: The control actions are discrete and include the following:  
1370 -move forward: control the robot to move forward for 0.5 meters.  
1371 -move backward: control the robot to move backward for 0.5 meters.  
1372 -stop: control the robot to stop moving.  
1373 -turn left: control the robot to move forward for 0.25 meters and turn left for 15  
1374 degrees.  
1375 -turn right: control the robot to move forward for 0.25 meters and turn right for  
1376 15 degrees.  
1377  
1378 Task Understanding:  
1379 1. **Goal bounding box:** This is provided by the user to indicate the expected  
1380 distance and angle between the target and the tracker, which is a bounding box  
1381 format, the agent should try to align the target bounding box with the goal  
1382 bounding box as much as possible.  
1383 2. **Target bounding box:** This is provided by user to indicate the current target  
1384 position in the image, in the bounding box format.  
1385  
1386 Task Definition:  
1387 Your task is to give a suitable action from Control actions, and try to align the Goal  
1388 bounding box with the target bounding box as much as possible.  
1389 1. **Actions:** Based on the given Goal bounding box and Target bounding box, you  
1390 should provide the best control action from the control actions to align the  
1391 target bounding box with the goal bounding box as much as possible.  
1392  
1393 Strategy Considerations:  
1394 The target bounding box size in the image represents the spatial distance, the smaller  
1395 size corresponds to a larger distance between the robot to the target.  
1396 If the center of the target bounding box is on the right side of the goal bounding box  
1397 center, the robot should turn right to align the target bounding box with the goal  
1398 bounding box. In contrast, if the center of the target bounding box is on the  
1399 left side of the goal bounding box center, the robot should turn left to align the  
1400 target bounding box with the goal bounding box.  
1401  
1402 Instructions: Given the provided target bounding box and goal bounding box, decide the  
1403 best action to adjust the robot's position.  
Provide ONLY and the increment of bounding box position and size in [output:] format in  
[Control Action] without additional explanations or additional text.

1392  
1393  
1394  
1395  
1396  
1397  
1398  
1399  
1400  
1401  
1402  
1403

Figure 12: System prompt used in baseline method GPT4-o.